A THESIS

ON

Halo structure of neutron drip line nuclei and related aspects

Dissertation submitted for the partial fulfilment of the requirement for

The award of the degree of

Master of Science

In

PHYSICS

Under the supervision of

Dr. Manoj Kumar Sharma

(Associate Professor)

Submitted by : **Silky Singla**

Roll no: 300904017

School of Physics and Material Science (SPMS)

Thapar University

PATIALA-147001 (Punjab)

July, 2011

DEDICATED TO:

GOD

AND

MY LOVABLE PARENTS

CERTIFICATE

This is to certify that Ms. Silky, Roll no. 300904017 has worked on this dissertation as a partial fulfilment for award of the degree of MASTERS OF SCIENCE in PHYSICS. I certify that the matter embodied in this report is of candidate's own record and not submitted to any other university in any part or full form for the award of such a degree.

Dr. Manoj K Sharma

Supervisor

School of Physics and Material Science (SPMS)

Thapar University, Patiala.

Countersignd by:

Dr. O. P. Pandey

(Prof. & Head)

School of Physics and Material Science

Thapar University,Patiala.

Dr. S. K. Mohapatra

Dean of Academic Affairs

Thapar University, Patiala.

ii

Acknowledgement

I owe my deepest gratitude to Dr. Manoj Kumar Sharma, *my worthy supervisor*, without him the dissertation would not have been possible. I thank him for the patience and encouragement that carried me on through difficult times, and for his insights and suggestions that helped to shape my research skills. I express my sincere thanks to him for his valuable guidance in caring out under his effective supervision, encouragement and cooperation. His visionary thoughts have influenced me greatly. His dynamical attitude has empowered me with zeal of energy to conquer the miner details of my research work.

I also thank Dr. O. P. Pandey, Professor & Head, School of Physics and Material Science for his support and providing facilities.

A special word of thanks to Ms. Gudveen Sawhney, a research scholar, for the help and valuable suggestions whenever I need it out of her busy schedule.

Special thanks to all my friends and the staff at the school of physics and material sciences for providing me a friendly atmosphere and encouraging me throughout this work. I am deeply thankful to my family, their moral support and patient has fruit through completion of this thesis.

Silky Singla

Silky

Roll No: 300904017

Date: 15/7/11

Abstract

The ground state decay of a large number of neutron rich (n-rich) light nuclei near the neutron dripline is studied using the Cluster Core Model (CCM). The CCM model find its basis in the well known Quantum mechanical Fragmentation Theory (QMFT), which have been applied successfully to study the decay of nuclear systems in light, intermediate, heavy and superheavy mass region. The halo nature of possible neutron drip line nuclei is studied via the minima in potential energy surfaces (PES), which in turn correspond to the most probable configuration. In present work, the main emphasis is on the angular momentum and deformation & orientation effects on halo nuclei. It is of great interest to see that in what way the angular momentum and deformations and orientations effects of the decaying fragments influence the potential energy surface PES behaviour of these rare light nuclei. The role of angular momentum and deformations & orientations seem to affect the fragmentation path of halo nuclei near the dripline. In other words, the cluster+core configuration seem to influence with inclusion of angular momentum and deformation effects in some of the cases studied in present work. Such studies are of extreme importance as the halo nuclei are used in break up reactions besides being used as the radioactive ion beams as a projectile because these nuclei are very loosely bound, unstable and have short half-life periods. The work carried out in this work seems highly relevant in context of present day developments in nuclear physics at low energies and could provide handful information for the further research work in the area of these lighter neutron rich nuclei near the dripline.

The introduction of neutron drip line halo nuclei is given in chapter 1. The methodology used (CCM) in the present work is given in chapter 2 and the results are discussed in chapter 3.

INDEX

Contents ***Page No.***

Certificate ----------ii

Acknowledgement ----------iii

Abstract ----------iv

List of figures ---------- vii

List of Tables ---------- viii

CHAPTER-1 ----------1-17

1.1 Nuclear Landscape ----------1

1.2 Halo ----------2

1.3 Classification of halo nuclei ----------5

(a) Neutron halo ----------5

(b) Proton halo ----------6

1.4 Evidences for halo structure ----------7

1.4.1 Structure Models ----------8

(a) Two-Body Systems

(b) Three-Body Systems – The Borromeans

1.4.2 Microscopic models ----------10

1.4.3 Reaction models ----------11

1.5 Interaction cross-section and radius for halo nuclei ----------11

1.6 Applications of Halo in breakup reactions ----------12

1.7 Nucleus and their shapes ----------14

1.7.1 Quadrupole deformation ----------15

1.7.2 Deformation parameters ----------15

References ----------16

CHAPTER-2 METHODOLOGY ----------18-27

2.1 Introduction ----------18

2.2 The (nucleon) Cluster Core Model (CCM) ----------18

2.3 Quantum Mechanical Fragmentation Theory ----------19

2.4 The Fragmentation potential $V(A_1, A_2, R, l)$ ----------20
2.4.1 Binding energy ----------21
2.4.2 The Proximity Potential for deformed, oriented and coplanar nuclei ----------23
2.4.3 The Coulomb potential ----------24
2.4.4 Rotational Energy due to angular momentum ----------24
References ----------26

CHAPTER-3 ----------28-52
3.1 Calculations and Discussion ----------28
3.1.1 One Neutron (1n) halo nuclei ----------30
3.1.2 Two Neutron (2n) halo nuclei ----------40
3.2 Summary ----------51
References ----------52

List of figures

Fig. 1.1 The neutron and proton driplines.

Fig. 1.2 Halo structure for a nucleus.

Fig. 1.3 some examples of neutron and proton halo nuclei near the driplines.

Fig. 1.4 represents the neutron halo nuclei.

Fig. 1.5 represents the 1p-halo nuclei.

Fig. 1.6 shows the extended radius value for ^{11}Li.

Fig. 1.7 shapes of nucleus

Fig. 2.1 Schematic configurations of two (equal/unequal) axially symmetric deformed, oriented nuclei, lying in the same plane and for various θ_1 and θ_2 values in the range 0^0 to 180^0.

Fig. 3 represents the graphs of various nuclei e.g. the nuclei ^{11}Be, ^{14}B, ^{15,17,19}C, ^{22}N, ^{22,23,24}O, ^{24,26,}F, ^{29}Ne and ^{31}Ne for 1n-halo nuclei and nuclei ^{6}He, ^{8}He, ^{11}Li, ^{12,14}Be, ^{17,19}B, ^{22}C, ^{23}N, ^{27}F and ^{29}F for 2n-halo nuclei.

List of Tables

Table 1.1 Interaction cross section of one- and two-neutron halo nuclei (N), of their core (C), difference between them and one- or two-neutron removal cross section.

Table 1.2 Two-neutron removal cross sections for ^{11}Li on different targets at an energy of 80A MeV.

Table 3.1 The calculated 1n-halo characteristics of light neutron-rich nuclei containing neutron separation energies.

Table 3.2 The calculated 2n-halo characteristics of light neutron-rich nuclei containing neutron separation energies.

Table 3.3 Magic character of the core nucleus of some observed and theoretically possible 1n- halo nuclei.

Table 3.4 Magic character of the core nucleus of some observed and theoretically possible 2n- halo nuclei.

Chapter 1

1.1 Nuclear Landscape

Among the available nuclei listed in nuclear charts only a limited number of nuclei exist. An arbitrary combination of protons and neutrons does not necessarily yield a stable nucleus. The heaviest stable isotope is ^{209}Bi and all heavier nuclides decay mainly by α-particle emission or even via spontaneous fission. There are no naturally-occurring nuclei on earth which undergo proton emission or neutron emission. This type of nuclei can be created in the laboratory with accelerators or naturally in stars. These particle decays are not commonly known because particle decay is governed by the nuclear strong force, as well as the Coulomb force in the case of charged particles, the duration of these decay transmission is of the order of femtoseconds or less. The addition of more nucleons (neutrons or protons) generally results in the decay of the nucleus. The newly-formed nucleus essentially undergoes immediate decay and the emitted nucleon is of the same isospin quantum number as that of the extra added nucleon i.e. proton or neutron. The nucleons are supposed to be 'leaked' or 'dripped' out of the target nucleus, hence giving rise to the term "drip line". If a neutron or proton is decaying from parent nucleus then the nuclei come into the neutron or proton dripline respectively. The neutron and proton driplines are shown in Fig.1.1

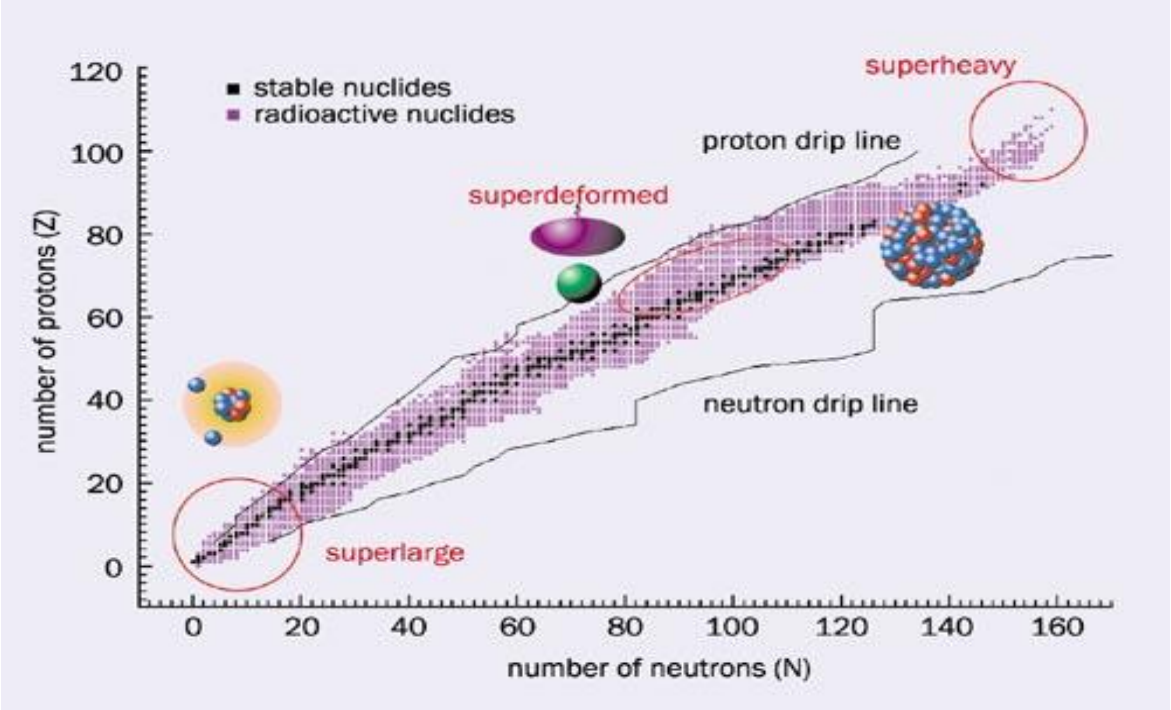

Fig. 1.1 shows the neutron and proton driplines.

The neutron drip line is generally depicted in for of a graph between atomic number (Z) and neutron number (N). In nuclear drip line number of neutrons are increasing on the abscissa and number of protons increasing along the ordinate. The neutron drip line serves as the neutron-rich boundary beyond which neutron-rich nuclei are unstable against neutron emission. The proton drip line, in contrast, serves as the opposite boundary of nuclear stability. The neutron-rich (n-rich) or proton-rich (p-rich) nuclei are mostly found near these driplines.

The neutron and proton halo nuclei are also neutron-rich (n-rich) and proton-rich (p-rich) nuclei respectively. The nucleons in halo nuclei are loosely bound from the core and hence they can easily emit neutron(s) and proton(s) from the nucleus. The field of halo nuclei represents a paradigm shift in the study of nuclear structure and is still regarded as a `hot' topic almost twenty years after their discovery. In our present work we have studied some nuclei near these neutron and proton driplines by using cluster-core model (CCM) [1-2] which find its basis in Quantum Mechanical Fragmentation Theory, discussed in chapter 2.

1.2 Halo

Broadly speaking on atomic nucleus is supposed to be made up from protons and neutrons as a liquid drop. But this is not always true. Researchers has found that some of constituents neutrons or protons form a misty cloud or halo, similarly as the electrons form a cloud around the nucleus to make atom. In a nucleus neutrons and protons i.e. nucleons attract each other, but only protons and neutrons can bind to each other in pairs called deuterons. The nuclei that contain equal no. of neutrons and protons are called stable nuclei. These nuclei occur naturally on earth.

The halo is a *threshold* effect arising from the very weak binding of the last one or two valence nucleons (usually neutrons) to, decoupling from, a well-defined inert ‘core’ containing all the other nucleons.

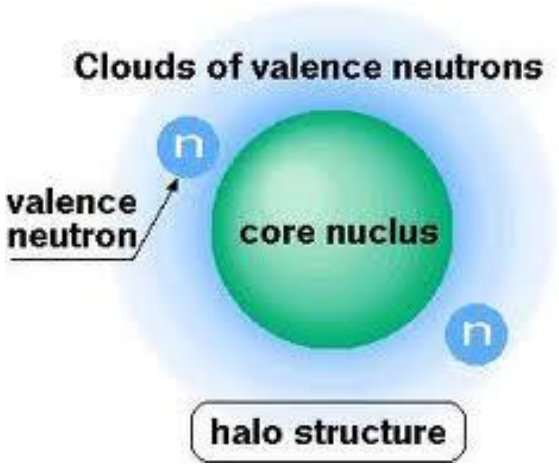

Fig. 1.2 Halo structure for a nucleus.

Fig.1.2 shows the halo structure for a nucleus in which the valence nucleons are loosely bounded around the core.

This definition emphasises the three main halo characteristics.

(i) Halo nuclei exhibit a strong cluster structure. That is to say, they are well described as a core plus one or two neutrons.
(ii) Halo nuclei have a large matter radius in comparison with the range of the nuclear interaction. This is explained in the few-body model by the fact that the halo neutrons have a high probability of being at a large distance from the core. The wave function of these nuclei is assumed to tunnel far outside the classically allowed region. This region corresponds to the positions the halo neutrons would occupy if their relative motions to the core were treated classically
(iii) Halo nuclei are weakly bound, i.e. the separation energy of the halo neutrons is very low. This two or three-body structure can therefore be easily broken.

The discovery of halo nuclei dates back to the mid-eighties, when laboratories became able to create and accelerate radioactive ion beams. It has been found that some very neutron-rich nuclei exhibit an astonishingly large matter radius in comparison with their close neighbours. The field of halo nuclei has generated much excitement and many hundreds of papers. Earlier β- and γ-decay studies of many of these types of nuclei yielded information about their lifetimes and certain features of structure but the measurement of the very large interaction cross sections of certain neutron-rich isotopes of helium and lithium was discovered in 1985

by Tanihata [3-4]. The first halo nucleus produced in the laboratory was ^{6}He, as long ago as 1936, using a beam of neutrons on a ^{9}Be target [5] a few years after the discovery of the neutron.

The strangeness of halo structure is that the valence neutrons have a very high probability of presence at a large distance from the core, far beyond the nuclear- interaction range. This means that they are tunnelling well outside the classically allowed region. Therefore they constitute a sort of halo surrounding the core. Quantum mechanics states that the combination of weak binding and short range nuclear force (since the core is relatively compact) means that the neutron(s) can tunnel out into a volume well beyond the nuclear core and into the 'classically-forbidden' region. One can consider the eigenfunctions of a particle bound in a finite 1-D square well potential. Deeply-bound states are mostly confined within the potential and have very little extension beyond its walls. But states having eigen-energies just below the surface of the well will have slowly decaying exponential tails extending well beyond the range of the potential. Quantum mechanically, this means that there is a significant probability of finding the particle outside of the well.

In halo nuclei, the potential well corresponds to the mean field potential of the rest of the nucleons in the nucleus. According to the Uncertainty Principle bound states have a relatively short lifetime, of the order of a few milliseconds to a few seconds. But this is quite long enough for these halo nuclei to be formed and used in nuclear reactions in order to study their unusual features.

Special feature of halo nuclei is that most halos tend to be manifest in the ground states of the nuclei. Indeed, most of the known halo nuclei tend to only have one bound state; any excitation of such a weakly bound system tends to be into the continuum, with the notable exception of ^{11}Be which has two bound states. But many nuclei will have excited states just below the one-neutron breakup threshold that exhibit halo-like features. After all, if the only criterion is that of weak binding then surely excited state halos would be everywhere. However, this is not the case. In addition to weak binding criteria the core nucleons must be tightly bound together and spatially decoupled from the valence neutron. The three most studied halo nuclei were ^{6}He, ^{11}Li and ^{11}Be. Many more others halo nuclei have also been confirmed. For example: ^{14}Be, ^{14}B, ^{15}C and ^{19}C. Actually we have a variety of neutron and proton halo nuclear systems in the light mass region. Fig 1.3 shows some of the well known neutron and proton halos near the dripline.

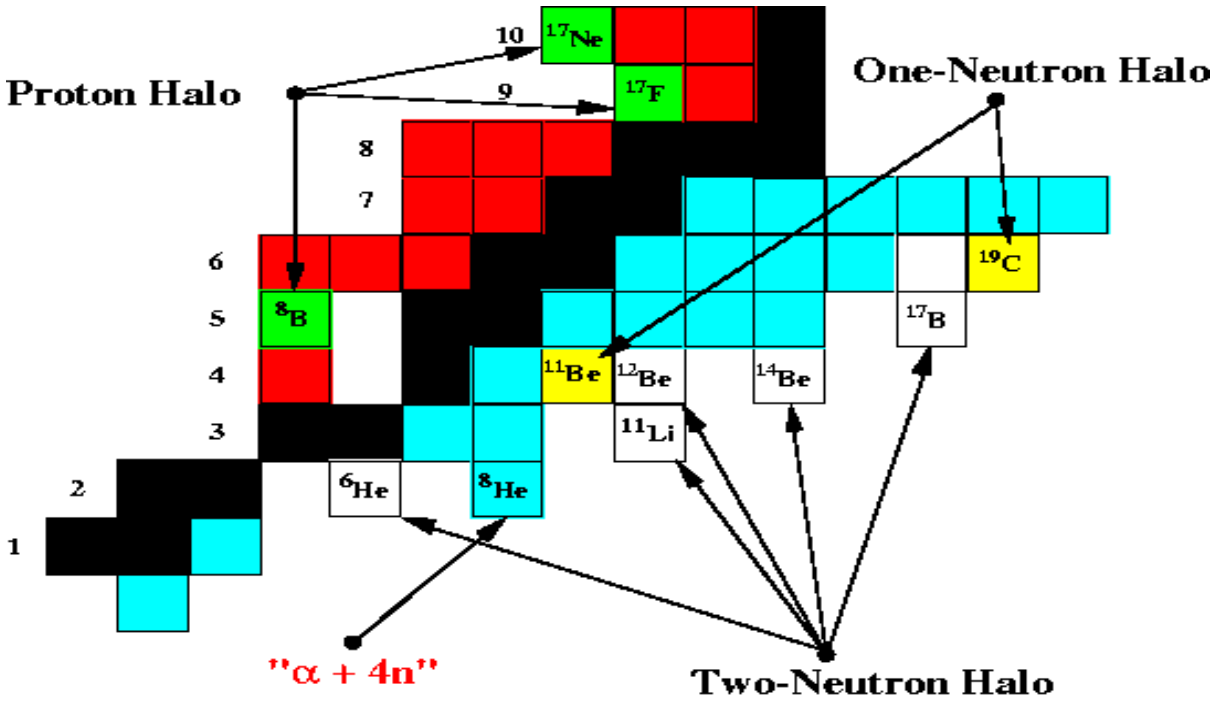

Fig 1.3 shows some examples of neutron and proton halo nuclei near the driplines.

1.3 Classification of halo nuclei

(a) Neutron halo

(b) Proton halo

(a) Neutron halo:

The development of radioactive nuclear beams in the mid-eighties enabled physicists to study nuclei far from stability [3-4]. This led to the discovery of neutron halo nuclei. The outermost neutrons extend outward from a nucleus and form a neutron halo. ^{11}Li is the first observed neutron halo. This is a ^{9}Li nucleus with 2 additional halo neutrons and this nucleus is large as ^{208}Pb nucleus. This is the most fragile nucleus. Other neutron halo nuclei are ^{6}He, ^{11}Li, ^{11}Be, ^{14}B, ^{19}C, ^{22}C, ^{23}N, ^{24}F, ^{27}F, ^{29}Ne etc. The separation energy of the last nucleon(s) becomes extremely small for nuclei near the drip line as compared with the common 6–8 MeV in stable nuclei. Many dripline nuclei have a nucleon or a two-nucleon separation energy in the range of 1-2 MeV. The neutron density distribution in such loosely bound nuclei shows an extremely long tail.

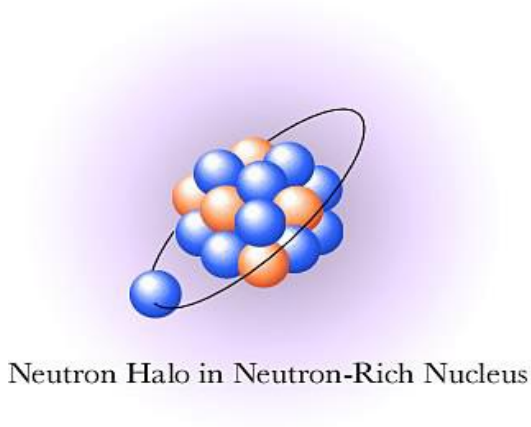

Fig 1.4 shows the neutron halo nuclei. The neutron is loosely bound to the core in this Fig. and form a neutron halo structure.

The two-neutron halo nuclei are called as borromean nuclei. In Borromean nuclei the knockout of a valence neutron is a process with high probability. The remaining subsystem of the core with only one neutron is unbound. These nuclei exhibit a three-cluster structure in which none of the binary subsystems are bound. For example ^{11}Li is bound though neither ^{10}Li nor dineuton exist.

(b) Proton halo:

The proton halos are those which have large quadrupole moment. As proton has charge so they repel each other whereas neutron does not have any charge. Proton halo nuclei are not quite as impressive in terms of the extent of their halo, due to the confining Coulomb barrier which holds them closer to the core.

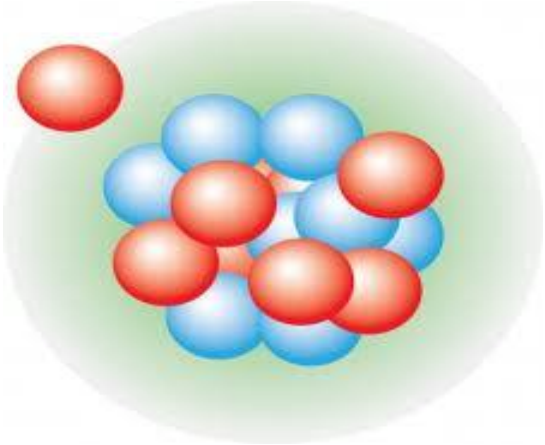

Fig. 1.5 shows the 1p-halo nuclei. The proton is loosely bound to the core and it forms a proton halo structure.

Decoupling of core and valence particles and their small separation energy are the important criterion for a halo and in addition to these there is one another criterion that the valence particle must be in a relatively low orbit angular momentum state, preferable an *s*-wave, relative to the core, since higher *l*-values give rise to a confining centrifugal barrier. The confining Coulomb barrier is the reason for proton halos not so extended as neutron halos.

1.4 Evidences for halo structure

In reference to halo structure, the first hint came from the measurement of the electric dipole transition between the two bound states in ^{11}Be. Firstly, a simple shell model picture of the structure of ^{11}Be suggested that its ground state should consist of a single valence neutron occupying the $0p_{1/2}$ orbital (the other six having filled the $0s_{1/2}$ and $0p_{3/2}$ orbitals). But it was found that the $1s_{1/2}$ orbital drops down below the $0p_{1/2}$ and this 'intruder' state is the one occupied by the neutron, making it a $(½)^+$ ground state. The first excited state of ^{11}Be, and the only other particle bound state, is the $(½)^-$ state achieved when the valence neutron occupies the higher $0p_{1/2}$ orbital. The very short lifetime for the transition between these two bound states was measured in 1983 [6] and corresponded to an E_1 strength of 0.36 W.u. It was found that this large strength could only be understood if realistic single particle wave functions are used to describe the valence neutron in the two states, which extended out to large distances due to the weak binding.

In the mid-1980's, the Berkeley experiment was carried out by Tanihata and his group. The interaction cross sections of Helium (He) and Lithium (Li) isotopes were measured and they found that the value is much larger than expected for the cases of ^{6}He and ^{11}Li. These corresponded to larger rms matter radii than that is predicted by the normal $A^{1/3}$ dependence. After two years, Hansen and Jonson [7] proposed that the large size of these nuclei is due to the halo effect. They explained the large matter radius of ^{11}Li by treating it as a binary system of ^{9}Li core plus a di-neutron. Dineutron is a hypothetical point particle, implying the two neutrons are stuck together i.e. the n-n system is unbound. Hence they showed that the weak binding between this pair of clusters could form an extended halo density.

During the late eighties and early nineties, both theorists and experimentalists were satisfied with simple estimates of various halo properties by reproducing experimental reaction observables like total reaction and Coulomb dissociation cross sections and momentum

distributions following nuclear breakup. Many models and formulae were used to calculate certain observables and some of these models are described here.

1.4.1 Structure Models

(a) Two-Body Systems

The general features of one-neutron halo nuclei can be studied using a simple 2-body (cluster) model of core + valence neutron bound by a short range potential. If the internal degrees of freedom of the nucleons in the core are decoupled from the single remaining valence neutron then we can simplify the many-body nuclear wave function,

$$\Phi_A \approx \varphi_{\text{core}}(\xi)\,\psi(\vec{r}) \tag{1.1}$$

where ξ denotes the core's intrinsic coordinates and $\psi(\vec{r})$ is the bound state wave function of relative motion of core and valence neutron. The total probability for the neutrons to be found outside the range of the potential is greater than the corresponding probability within the potential (i.e. the neutron is most likely to be found beyond the reach of the potential that is binding it to the core) is one criterion for a halo state to exist. These simple models of one-neutron halo nuclei in terms of the neutron's single particle wave function are not accurate enough to account for the physics that can now be accurately measured experimentally.

(b) Three-Body Systems – The Borromeans

The ^{6}He can be modeled as a bound three-body $\alpha + n + n$ system despite there being no bound states of α+n (^{5}He) or n+n (the dineutron). These nuclei have been dubbed 'Borromean' [8]. The wavefunctions of these nuclei requires special asymptotic features to account for this behavior. The relative motion of the core and two neutrons is defined in terms of the Jacobi coordinates ($\vec{x}$, $\vec{y}$). An extension of the one-neutron halo case suggests we can once again simplify the full many-body wavefunction by writing

$$\Phi_A \approx \varphi_{\text{core}}(\xi)\,\psi(\vec{x}, \vec{y}), \tag{1.2}$$

where the relative wave function, ψ, is a solution of a three-body Schrodinger equation. It is a non-trivial problem to calculate ψ, one can nevertheless decrease this 6-D equation to a one-dimensional 'radial' equation using hyper spherical coordinates (ρ, α, θ_x, ϕ_x, θ_y, ϕ_y) where $\rho = x^2+y^2$ is the *hyper radius* and $\alpha = \tan^{-1}(x/y)$ is the hyper angle [9].

The hyperradius, ρ, depends on the magnitudes of both Jacobi coordinates. Therefore it provides a useful measure of the extent of the halo for the case of Borromean nuclei. The overall matter radius of such systems is defined as

$$< \boldsymbol{r^2} > = \frac{\mathbf{1}}{\boldsymbol{A}}((\boldsymbol{A}-\mathbf{2}) < r_{core}^2 > + < \boldsymbol{\rho^2} >$$

Where $\langle r^2 \rangle_{core}$ is the intrinsic mean square radius of the core. For example in ^{11}Li the radius of ^{9}Li is 2.3 fm while the root mean square hyperradius, describing the relative motion of the valence neutrons relative to the core, about 9 fm. Together, these give a mass-weighted overall radius for ^{11}Li of about 3.5 fm.

This approach is not too much sensible for defining the size of a halo nucleus. No one would suggest that the size of an atom be defined as the mass weighted sum of the sizes of its electron cloud and its nucleus. That's why many accounts of halo nuclei describe ^{11}Li as being the same size as a lead nucleus rather than, ^{48}Ca, which also has a radius of about 3.5 fm (shown in fig 1.6)

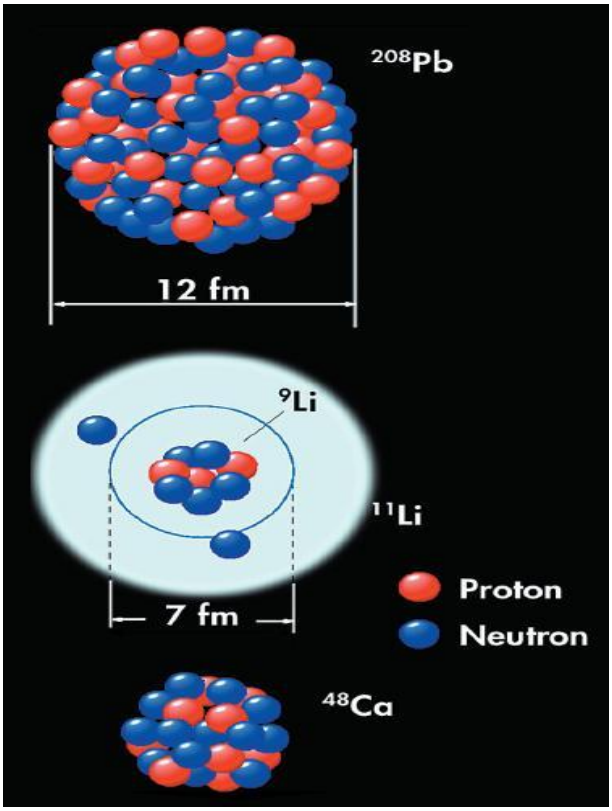

Fig.1.6 shows the extended radius value for ^{11}Li.

A number of elaborate techniques have been used to calculate the threebody wavefunctions of Borromean nuclei [10-15]. All these approaches assumed two-body pair wise potentials between the three constituents. It is important to treat the three-body asymptotic behaviour of the wavefunctions correctly in order to reproduce the basic features of these nuclei as well as the various reaction observables.

1.4.2 Microscopic models

Projecting the full many-body wavefunction onto two- or threebody model spaces as done in (1.1) and (1.2) is just an approximation. The few-body models of the structure of halo nuclei suffer from several shortcomings, namely anti symmetrisation. It is often treated only approximately and the excitation and polarisation effects of the core are ignored, although a number of studies are in progress to improve on these deficiencies. A number of studies are developing fully microscopic (*ab initio*) structure models. These are fully antisymmetric, start from a realistic NN interaction and could even include 3-body forces. The standard shell model fails to describe many of the essential features of halo nuclei beside that it proves spectroscopic information on a number of exotic nuclei and many theorists acknowledge that there is a real need to go beyond the conventional shell model. Then the Continuum Shell Model and Gamow Shell Model [16] are showing promising early results. For very light systems, progress is being made with the No-Core Shell Model [17], and the hope is that there will be a convergence of these two methods. But the question is, will they be able to predict a matter radius for ^{11}Li of 3.5 fm?

The Greens Function Monte Carlo method (GMC) [18] is another microscopic structure model for a halo state to exist. This approach involves calculating an approximate *A*-body wavefunction using the variational Monte Carlo method then using Greens function projection methods to obtain the desired bound state wavefunction. The GMC method has been applied to describe the bound states of nuclei up to $A = 12$, including the halo states. However, as we go to higher system it has some problems. Another promising approach is the Coupled Cluster Method [19]. This has been used widely in a number of other fields such as chemistry and atomic and condensed matter physics and has only been applied seriously to nuclear structure. In its early stages, it has been tested successfully against GMC for ^{4}He. It has been predicted that it will be more successful in reaching heavier dripline nuclei than GMC.

1.4.3 Reaction models

Halo nuclei are short lived (less than a second) they cannot be used as a nuclear target. Therefore, experiments are performed in inverse kinematics, where a beam of exotic nuclei hits a stable target. Such simple models can impart important information, if the reaction conditions are worked out properly. In reactions involving halo nuclei, it is important to note that the few-body correlations that are built into these structure models have to be retained. The important consideration in the study of reactions with halo nuclei is that they are easily broken up in the nuclear and Coulomb fields of the target nucleus. Therefore, excitations of the halo nucleus into the continuum must be included in the reaction model.

1.5 Interaction cross-section and radius for halo nuclei

The first value that has been measured on exotic nuclei using secondary radioactive beams is the interaction cross section (σ_1) [3-4]. It is defined as the total cross section for all processes in which the projectile number of nucleons is changed. From the interaction cross sections, one can define, the interaction radius [3] using a simple geometrical model,

$$\sigma_1 (P, T) = \pi (R_I (P) + R_I (T))^2$$

where P is set for projectile and T for target. It has been shown that the interaction radius is more or less independent of the target [3-4].

Measuring the interaction cross sections for different targets one can obtain the interaction radius of a projectile. In nuclear theory, it is known that stable nucleus density is rather constant up to a certain radius from which it drops to zero. The central density is quite similar from the lightest nuclei to the heaviest. This led to the semiclassical liquid-drop model in which nuclei are viewed as liquid droplets with a homogeneous density. In this model, a nucleus containing A nucleons is therefore seen as a sphere with a radius R proportional to $A^{1/3}$

$$R = r_0 A^{1/3} \qquad (1.3)$$

with $r_0 \approx 1.2$ fm.

If one assumes that the interaction radius is somehow a measure of the nuclear size, it should follow the $A^{1/3}$ law predicted from the liquid-drop model. Some nuclei near the neutron drip line (like ^{6}He, ^{8}He, ^{11}Li, ^{11}Be or ^{14}Be) exhibit anomalously high interaction radii in

comparison with their neighbours. This indicates that those nuclei have large nuclear radii due to an extended matter density and/or a major deformation [4].

1.6 Applications of Halo in breakup reactions

In breakup reactions, the nuclear and Coulomb interaction between halo and target takes place and as a result the halo dissociates from the core. The study of halo breakup can therefore convey information about the halo structure. This reaction turns out to be very likely in collisions including a halo nucleus. Fragment cross sections were measured [20] for a two-neutron halo projectile ^{11}Li on a C target at 790A MeV energy. They found higher cross section for production of the ^{9}Li than for any other fragment of the projectile. This reaction corresponds to two-neutron removal and its large cross section is qualitatively understood as a high probability of the removal of the loosely bound halo neutrons.

Using a Glauber-type model in which the halo structure of ^{11}Li was taken into account, Ogawa et al. [21] have shown that the two-neutron removal cross section (σ_{2n}) was equal to the difference between the ^{11}Li and ^{9}Li interaction cross section with target T.

$$\sigma_{2n}(^{11}\text{Li, T}) = \sigma_1\ (^{11}\text{Li, T}) - \sigma_1\ (^{9}\text{Li,T}) \qquad (1.4)$$

The one or two neutron removal cross sections have been measured for one or two-neutron halo nuclei respectively. They have been compared with the interaction cross section of the nucleus and that of the core. It has been found relatively good agreement with (1.4). Table 1.2 displays values for ^{11}Be and ^{11}Li nuclei with a C target at 790A MeV.

Nucleus	Core	σ_I(N)	σ_I(C)	σ_I(N) − σ_I(C)	σ_n(N) or σ_{2n}(N)
^{11}Be	^{10}Be	942 ± 8	813 ± 10	129 ± 18	169 ± 4
^{11}Li	^{9}Li	1047 ± 40	796 ± 6	251 ± 46	213 ± 21

Table 1.1: Interaction cross section of one- and two-neutron halo nuclei (N), of their core (C), difference between them and one- or two-neutron removal cross section. Cross sections have been measured for C target at energy of 790A MeV and values are expressed in mb and are taken from Refs. [4, 20, 21, 23].

The measurements were performed by using light targets. In these types of reactions, the Coulomb interaction is negligible. In order to study the importance of the nuclear and Coulomb interactions in the halo breakup, experiments have been conducted. Blank et al. [24] have measured the σ_{2n} for ^{11}Li on both light and heavy (high Z) targets (Table 1.2). The nuclear contribution σ^{N}_{2n} was calculated with the eikonal model of Bertsch et al. [25]. The Coulomb contribution σ^{C}_{2n} to the dissociation was obtained by subtracting σ^{N}_{2n} from σ_{2n}:

The proportion of the Coulomb contribution to σ_{2n} increases, as expected, with the target proton number. Being negligible for light C target, it becomes the most frequent dissociation process for heavy Pb target. The Coulomb halo breakup can therefore be another source of information about halo structure.

Target	σ_{2n}	σ^{N}_{2n} (calculated)	σ^{C}_{2n} (deduced)
C	170^{+30}_{-30}	235	-70^{+30}_{-30}
Sn	1090^{+290}_{-220}	584	510^{+290}_{-220}
Pb	1970^{+230}_{-300}	698	1270^{+230}_{-300}

Table 1.2 Two-neutron removal cross sections for ^{11}Li on different targets at an energy of 80A MeV. The nuclear part σ^{N}_{2n} of the cross section was calculated following [25], and the Coulomb contribution σ^{C}_{2n} was deduced by subtracting σ^{N}_{2n} from σ_{2n}. The values are expressed in mb and taken from Ref. [24]

In our present work we have studied the structure of these neutron and proton halo nuclei using the Cluster Core Model (CCM) based on collective clusterization process and discussed in chapter 2. We have studied the ground state decay of a variety of halo nuclei using CCM.

The main aim of the present work is to see the effects of nuclear deformation and orientations on the fragmentation path of halo nuclei. The associated angular momentum effects are also addressed. Such study could be useful as an extensive work is being done on these exotic nuclear systems in recent times [26, 27, 28]. The details of calculations are given in chapter 3. As the deformation and orientation effects are studied in reference to halo, so a brief account of nuclear deformation effects is given in the next section.

1.7 Nucleus and their shapes

Nuclei can be both spherical and deformed in their ground state. In many respects spherical nuclei are exceptional, and majority of nuclei are deformed. Many nuclei are only slightly non-spherical, so they can be well described by spherical nuclear models. The deformation and orientation contributions become extremely important & need to be incorporated explicitly in order to account for nuclear dynamics.

A nucleus with a completely filled shell of either protons or neutrons is said to be magic because it is relatively more stable than nuclei with either a larger or a smaller number of nucleons. Most of magic nuclei are spherical in shape, but some nuclei can lower their energy somewhat, and hence increase their stability, by rearranging their protons and neutrons into deformed shells accommodating a different number of nucleons. Most commonly, the protons and neutrons each form a series of concentric shells to give the nucleus a spherical or near-spherical shape (left part of Fig.1.7). However, in some nuclei the outermost neutrons and protons move with respect to the inner protons and neutrons and the result is a "highly deformed" shape (center part of Fig.1.7), in which the length is about 1.5 times greater than its width. In even more extreme cases, "superdeformed nuclei" can result (right part of fig.1.7); with length width ratio of about 2:1 with a nucleus with a completely filled shell of either protons or neutrons.

Fig. 1.7 shapes of nucleus

To begin with a nucleus is considered to have spherical shape, but if the distribution of charges in the nucleus is not spherically symmetric, the nucleus will have quadruple moment. The single particle states of quadrupole deformed nuclei are described by the Nilsson model [29]. Deformation alters the properties of single-particle wavefunctions from those of the spherical shell model. The breaking of spherical symmetry changes the degeneracies of energy levels, and allows for collective rotation of the nucleus. When the charge distribution

is not spherical, deformed nuclei can have large electric multipole moments. The presence of rotational excited states and the detection of large quadrupole moments are good indications that a nucleus is deformed. Quadrupole moment measures the departure of nucleus from its spherical symmetry. The quadrupole moment of a spherically symmetric nucleus is zero.

To lowest order, most deformed nuclei can be approximated as quadrupole deformed i.e. a prolate or oblate ellipsoid. Higher order deformations, such as octupole and hexadecapole are also possible, as are triaxial deformations and other more exotic shapes.

1.7.1 Quadrupole deformation

A quadrupole deformed nucleus has a prolate or oblate ellipsoidal shape. This is the lowest order deformation seen in nuclei. A prolate ellipsoid has two equal, short axes and a single long axis; an oblate ellipsoid has two equal long axes and one short axis. For deformed nuclei, the axis of unequal length is often termed the deformation axis.

1.7.2 Deformation parameters

The degree to which a nucleus is deformed is described by a deformation parameter: ε or β. ε is the deformation neck length parameter used in the Nilsson model for describing single particle properties of the nucleus, while β is used when describing collective behaviour such as rotation. In each case, a positive deformation parameter indicates a prolate shape while a negative deformation parameter describes an oblate shape.
If quadrupole moment is denoted by β_2 then the general formula for quadrupole moment is given by

$$\beta_2 = 2/5\ Z(b^2-a^2)$$

where Z is the atomic number of the nuclei and b and a are the semi major and semi minor axis of the nuclei

Most nuclei, however, tend to be deformed because their shells are only partially filled. According to the laws of quantum mechanics, the nucleus can coexist in different shapes (e.g. elongated and flattened) at the same time. A nucleus will prefer a deformed shape rather than a spherical shape in majority of cases where deformed configurations lead to relatively less energy or more stability zone.

References

[1] R.K. Gupta, S. Kumar and W. Scheid 1995 *J. Phys. G: Nucl. Part. Phys.* 21 L27

[2] R. K. Gupta, M. Balasubramaniam,R.K. Puri and W. Scheid 2000 *J. Phys. G: Nucl. Part. Phys.* 26 L23

[3] I. Tanihata et al., Phys. Lett. B 160, 380 (1985).

[4] I. Tanihata et al., Phys. Rev. Lett. 55, 2676 (1985).

[5] T. Bjerge, K.J. Borgstr¨om, Nature 138, 400 (1936).

[6] D. J. Millener, J.W. Olness, E.K. Warburton, S. Hanna, Phys. Rev. C 28, 497 (1983)

[7] P. G. Hansen, B. Jonson, Europhys. News 4, 409 (1987).

[8] M. V. Zhukov et al., Phys. Rep. 231, 151 (1993).

[9] J. Al-Khalil, Phys. 651, 77–112 (2004).

[10] M. V. Zhukov et al., Phys. Rep. 231, 151 (1993) .

[11] I. J. Thompson and M.V. Zhukov, Phys. Rev. C 53, 708 (1996).

[12] P. Descouvemont, Phys. Rev. C 52, 704 (1995).

[13] K. Varga, Y. Suzuki, Phys. Rev. C 52, 2885 (1995).

[14] Y. Kanada-En'yo, Hisashi Horiuchi, Akira Ono, Phys. Rev. C 52, 628 (1995).

[15] D.V. Fedorov, A.S. Jensen, K. Riisager, Phys. Rev. C 49, 201 (1994).))

[16] W. Nazarewicz, M. Ploszajczak, proceedings of this conference.

[17] P. Navr´atil, W.E. Ormand, Phys. Rev. Lett. 88 152502 (2002), and references therein.

[18] S.C. Pieper and R.B. Wiringa, Annu. Rev. Nucl. Part. Sci. 51, 53 (2001)

[19] D. J. Dean, M. Hjorth-Jensen, Red. Mod. Phys. 75, 607 (2003).

[20] T. Kobayashi et al. , Phys. Rev. Lett. 60, 2599 (1988)

[21] Y. Ogawa, K. Yabana, and Y. Suzuki, Nucl. Phys. A543 722 (1992)

[22] M. Fukuda et al. , Phys. Lett. B 268, 339 (1991)

[23] I. Tanihata et al. , Phys. Lett. B 206, 592 (1988)

[24] B. Blank et al. , Nucl. Phys. A555, 408 (1993)

[25] G. F. Bertsch, H. Esbensen, and A. Sustich, Phys. Rev. C 42,758 (1990)

[26] E. F. Agnilera et. al. , Phys. Rev. C 79, 021601 (R) 2009.

[27] A. Lemasson et. al. , Phys. Rev. Lett. 103, 232701 (2009).

[28] K. Tanaka et. al. , Phys. Rev. Lett. 104, 062701 (2010).

[29] Irvine, J. M. 1972, 'Nuclear Structure Theory', Pergamon Press, Oxford

Chapter 2

2.1 Introduction

The main aim of this work is to study the fragmentation process of halo nuclei using the modified (nucleon) Cluster Core Model (CCM) [1-2]. The concept of minima in potential energy surfaces (PES) is exploited to single out the most probable decaying fragments. It is important to note that deformations and orientation effects of the reaction partners and decay products are explicitly included together with temperature and angular momentum in this model. However our calculations are confined only for the ground state decay of parent nucleus i.e. at T = 0. Details of CCM are given in the section 2.2, which stem from the Quantum Mechanical Fragmentation Theory, (QMFT) [3-17] which in binary fragmentation, uses a collective mass transfer process discussed later in section 2.3. We calculate the fragmentation potential (discussed later in section 2.4) which is sum of the Binding energies, Coulomb potential, Proximity potential and rotational energy due to angular momentum for the all cluster+core configurations.

2.2 The (nucleon) Cluster Core Model (CCM)

This is a simple theoretical method of potential energy surfaces (PES), the cluster-core model (CCM), given by [1-2] for nucleon-rich light nuclei. This model was firstly referred to as (neutron) CCM. Then after sometime it was found that the method works equally well for proton-rich light nuclei as well, provided Coulomb energy of protons in proton-clusters is added. CCM is an important theoretical method for identifying the halo structure of n-or p-rich light nucleus, other than the hypothesis of (neutron or proton) separation energy discussed later in chapter 3. It may be noted that the cluster is here a general term, used not only the α-particle and heavier nuclei but also for one or two neutron (or proton). In the CCM, we calculate the potential energy surface (PES) of a nucleus for its all possible cluster+core (A_2 , A_1) configurations and look for a neutron(s)-cluster (or proton(s)-cluster) + core configuration with a minimum potential energy.

The potential energy used for a cluster + core configuration (A_2 , A_1) of a nucleus A is defined as sum of binding energies, Coulomb repulsion, additional attraction due to nuclear Proximity and rotational energy due to angular momentum. As mentioned earlier the effects of

deformations, orientations and angular momentum are explicitly included in the fragmentation potential, as given in Eq. 2.1.

We have calculated the all potential terms in Eq. (2.1) and then plotted these potential values as a function of mass number in order to find minima in PES. The binding energy for a cluster with *x* neutrons ($x \geq 1$) is taken to be *x* times that of the one-neutron binding energy (the one neutron mass excess $\Delta m_n = 8.0713\ MeV$) i.e.

$$B(A_2 = xn) = x\Delta m_n \qquad \text{(for neutron- clusters).}$$

for proton-clusters, we define the same as

$$B(A_2 = xp) = x\Delta m_p - a_c {A_2}^{5/3} \qquad \text{(for proton- clusters).}$$

with $\Delta m_p = 7.2880\ MeV$, the one-proton mass excess i.e. equivalent of the one-proton binding energy, and the mass excess $a_c = 0.7053$ MeV [18]. The additional term is the disruptive Coulomb energy $(= -a_c {Z_2}^2 / {A_2}^{5/3})$ between the protons (here $x = A_2 = Z_2$). According to the above definitions for binding energies of n- or p-clusters means the nucleons in these cluster are taken to be unbound, just as is the case in the model Hansen and Jonson [19].

2.3 Quantum Mechanical Fragmentation Theory

In QMFT [3-17], the essential quantities for the description of the nuclear dynamics are the potential energy surfaces and the mass parameters defining the kinetic energy of the system while the static properties of nuclear system are determined by the potential energy only. The QMFT is worked out in terms of the following collective variables:

(1) Relative separation coordinate R between the two nuclei or, in general two fragments (or, equivalently, the length parameter $\lambda = L/2R_0$, with L as the length of the nucleus and R_0, as the radius of an equivalent spherical nucleus).

(2) The deformation co-ordinates $\beta_{\lambda i}$ $(\lambda = 2,3,4 \ldots\ldots and\ i = 1,2)$ of the colliding nuclei.

(3) The orientation degrees of freedom θ_i $(i = 1,2)$of the deformed nuclei.

(4) Azimuthal angle ϕ between the principles planes of the two colliding nuclei.

(5) Neck parameter ε, defined by the ratio $\varepsilon = E_0 / E'$ for the interaction region ($R < R_1+R_2$, R_i $(i = 1,2)$ is the radius of the two nuclei);

Where E_0 is the actual height of the barrier and E' is the fixed barrier of the two centre oscillator. $\varepsilon = 0$ represents a broad neck formation, whereas ε= 1 gives that the neck is fully squeezed in, corresponding to the asymptotic region ($R > R_1 + R_2$)

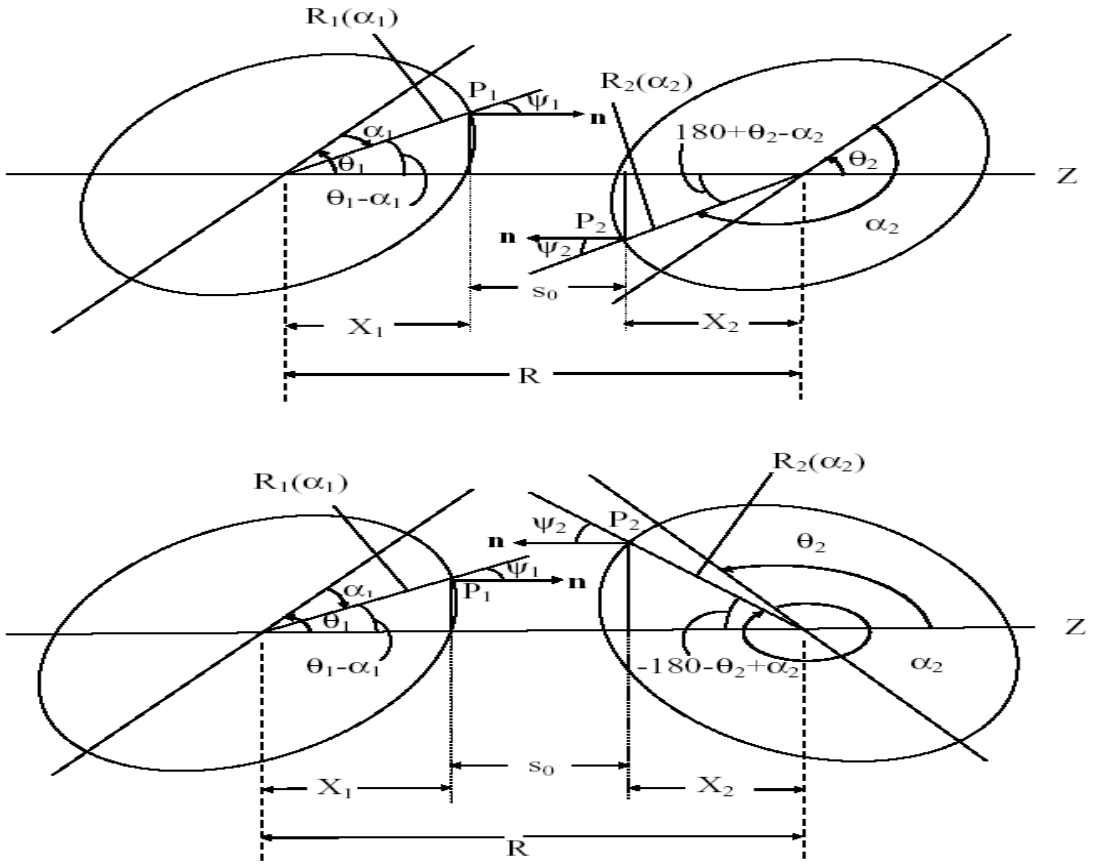

Figure 2.1 Schematic configurations of two (equal/unequal) axially symmetric deformed, oriented nuclei, lying in the same plane and for various θ_1 and θ_2 values in the range 0^o to 180^o. The θ's are measured in anti-clockwise from the colliding axis.

2.4 The Fragmentation potential $V(A_1, A_2, R, l)$

The collective potential energy or the fragmentation potential $V(A_1, A_2, R, l)$, is calculated as,

$$V(A_1, A_2, R, l) = \sum_{i=1}^{2}[B_i(A_i, Z_i, \beta_{\lambda i})] + V_c(R, Z_i, \beta_{\lambda i}, \theta_i, \phi) + V_P(R, A_i, \beta_{\lambda i}, \theta_i, \phi) + V_l(R, A_i, \beta_{\lambda i}, \theta_i, \phi) \quad (2.1)$$

Here B_i $(i = 1,2)$ are the binding energies of the two nuclei, available from the experimental data of Audi-Wapstra [20]. Wherever the experimental *B*'s are not available, the theoretical

binding energies of Moller et al. [21] are used. Note that the binding energies contain both the macroscopic (liquid drop part) and the microscopic (shell correction part). The halo structure in light nuclei at the drip lines could be explained on the basis of surface energy term in the liquid drop formula. The binding energy, the nuclear Proximity interaction energy V_P, the Coulomb potential V_C and centrifugal potential V_l are discussed later on (sections 2.4.1, 2.4.2, 2.4.3 and 2.4.4.). The charges Z_i in the above equation (2.1) of potential are fixed by minimizing the sum of two binding energies in Z_1 or Z_2. The shape of the potential $V(A_1, A_2, R, l)$ is independent of choice of value of R. We are using here only the touching configurations i.e. $R = R_1 + R_2 = R_t$. In general, we calculate value of R from the formula $R_i = R_0 \, A^{1/3}$, where R_0 is a constant value (1.15fm). But in case of halo the R_0 changes from nucleus to nucleus and from one isotope to another isotope. However, in our calculations, radius with the effects of deformation included is calculated as per the expression given below

$$R_i(\alpha_i) = R_{0i} \, [1 + \sum_\lambda \beta_{\lambda i} \, Y_\lambda^{(0)}(\alpha_i) \,], \tag{2.2}$$

and

$$R_{0i} = 1.28 \, A_i^{1/3} - 0.76 + 0.8 \, A_i^{-1/3} \tag{2.3}$$

Here $\lambda = 2,3,4$ .... and α_i is an angle that the radius vector R_i of the colliding nuclei makes with the symmetry axis (Fig.2.1).

2.4.1 Binding energy

Further, in Eq. (2.1), within the Strutinsky renormalization procedure [22], we have defined the binding energy *B* of a nucleus at temperature *T* as

$$B_i(A_i, Z_i, \beta_{\lambda i}, T) = \sum_{i=1}^{2} . V_{LDM}(A_i, Z_i, T) + \sum_{i=1}^{2} . \delta U \exp(-T^2/T^2_0) \tag{2.4}$$

For the study of excited systems, where the nuclear temperature effects also come into picture, the fragmentation potential at fixed R is

$$V(A_1, A_2, T) = \sum_{i=1}^{2} . V_{LDM}(A_i, Z_i, T) + \sum_{i=1}^{2} . \delta U \exp(-T^2/T^2_0) + V_c(Z_i, \beta_{\lambda i}, \theta_i, \varphi, T) + V_p(A_i, \beta_{\lambda i}, \theta_i, \varphi, T) + V_l(A_i, \beta_{\lambda i}, \theta_i, \varphi, T) \tag{2.5}$$

Here, $V_{LDM}(A_i, Z_i, T)$ is the liquid drop part of the binding energy and δU, the shell corrections. Note that the calculation of fragmentation potential involves all the possible decay channels and the number of all such possible decay channels becomes more and more with the increasing mass of the mother nucleus. The shell corrections δU in Eq. (2.4) are considered to vanish exponentially for $E^*_{CN} \geq 60$ MeV, giving $T_0 = 1.5$ MeV. At higher excitation energies the shell corrections vanish completely and only the liquid drop part of energy is present. The shell corrections play an important role in determining or empirical fitting of nuclear masses, because the nuclear masses calculated by using the smooth liquid drop formula show large deviations with respect to the experimental masses. It means that in the experimental masses there exist deep minima at specific neutron and/or proton numbers indicating the presence of shell structure, the so-called magic numbers in nuclei. This characteristic behaviour cannot be reproduced by the liquid drop part alone, which means that the introduction of microscopic shell correction in the mass formula is essential. Thus, shell corrections accounts for the removal of deviation from the liquid drop calculations (uniform distribution of nucleons), and are defined, within Strutinsky [22] method as

$$\delta U = U - \widetilde{U} \tag{2.6}$$

where, $U = \sum_\nu E_\nu 2n_\nu$ is the sum over all occupied single particle states and

$$\widetilde{U} = \int_{-\infty}^{\tilde{J}} E\tilde{g}(E)dE \tag{2.7}$$

is the average energy for uniform distribution. In general, the microscopic shell correction, together with the liquid drop part, gives a proper description of the binding energy of the nucleus. This method, however, does not give a proper description of light mass nuclei. The difficulty is the inadequacy of shell model for very light nuclei. For this reason, the macro-microscopic calculations of Moller *et al.* [21] are tabulated for $Z \geq 8$ only. For $Z \leq 8$, one could alternatively use the empirical shell correction method of Myers-Swiatecki [18] which again is not very satisfactory for light nuclei ($Z \leq 16$). Gupta and collaborators have modified this empirical method and obtained a better description of the shell corrections for the light as well as heavy mass region, i.e., $1 \leq Z \leq 118$ [23,26].

2.4.2 The Proximity Potential for deformed, oriented and coplanar nuclei

Whenever two surfaces approach each other within a small distance of less than ~ 2fm, comparable with the surface thickness of interacting nuclei, or when a nucleus is at the verge

of dividing into two fragments, then the two surfaces actually face each other across a small gap or crevice. In both cases, the surface energy term alone could not give rise to the strong attraction that is observed when the two surfaces are brought in close proximity. Such additional attractive forces are called Proximity forces and the additional potential due to these forces is called the nuclear Proximity potential. Blocki et al. [24] have reanalyzed and extended a theorem, originally due to Deryagin [25], according to which the force between two gently curved surfaces in close proximity is proportional to the interaction potential per unit area between the two flat surfaces. The original expression of Blocki based on the pocket formula was for spherical nuclei, and is given as

$$V_P(A_i\beta_{\lambda i}\theta_i\ T) = 4\pi\overline{R}(T)\gamma b(T)\phi(\ s_0(T)) \tag{2.8}$$

$\phi(\ s_0)$ is the universal function, independent of the shapes of nuclei or the geometry of nuclear system, but depends on the minimum separation distance s_0

$$\phi(\ s_0) = \begin{cases} -1/2(s_0\ -\ 2.54)^2 - 0.0852(s_0\ -\ 2.54)^3 \\ -3.437\exp(-s_0/0.75) \end{cases} \tag{2.9}$$

respectively, for $s_0 \leq 1.2511$ and $s_0 \geq 1.2511$. Here, s_0 is defined in units of b, i.e. s_0 is s_0/b. This function is defined for negative (the overlap region), zero (touching configuration) and positive values of s_0. The distance of closest approach, s_0, defined in (Fig.2.1), depends on deformations and orientations of reactants/products for a fixed R, the minimum distance s_0 for spherical nuclei is defined as

$$s_0 = R - R_1 - R_2 \tag{2.10}$$

where $R = 1.07\ A_i^{1/3}$(i=1,2). b is the diffuseness of the nuclear surface given by

$$b=[\pi/2\sqrt{3}\ln 9]\ t_{\ 10-90} \tag{2.11}$$

where $t_{\ 10-90}$ is the thickness of the surface in which the density profile changes from 90% to 10%. The value of b ~1 fm. Here the temperature dependent b is given as

$$b(T) = 0.99(1+0.00T^2)$$

The γ is the specific nuclear surface tension given by

$$\gamma = 0.9517\ [1-1.7826(\tfrac{N-Z}{A})^2\ ]\ \text{MeV}\ fm^{-2} \tag{2.12}$$

$\overline{R}$ is the mean curvature radius of the reaction partners which for spherical nuclei is given by Eq. (2.13) and for deformed and oriented nuclei is described in the Fig. 2.1

$$\overline{R} = R_1 R_2/(R_1 + R_2) \tag{2.13}$$

Fig.2.1 shows a schematic configuration of two (equal/ unequal) axially symmetric deformed, oriented nuclei, lying in the same plane ($\phi = 0°$), for various θ_1 and θ_2 values in the range 0° to 180° . θ_i is the angle of orientation, defined as an angle between the symmetry axis and the axis of collision, with its rotation measured in anti-clockwise direction from the axis of collision. α_i is an angle between the symmetric axis and the radius vector R_i (α_i ; T) of the colliding nuclei, measured in clockwise direction from the symmetry axis of the nucleus.

2.4.3 The Coulomb potential

Coulomb potential describes the force of repulsion between two interacting nuclei due to their charges. It acts along the line joining the two nuclei. The Coulomb potential for two interacting hot, deformed and oriented nuclei is given in Eq. (2.14)

$$V_c(Z_i, \beta_{\lambda i}, \theta_i, T) = \frac{Z_1 Z_2 e^2}{R(T)} + 3Z_1 Z_2 e^2 \sum_{\lambda,i=1,2} \frac{R_i^{\lambda}(d_i,T)}{(2\lambda+1)R(T)^{\lambda+1}} \times Y_{\lambda}^{(0)}(\theta_i)\left[\beta_{\lambda i} + \beta_{\lambda i}^2 Y_{\lambda}^{(0)}(\theta_i)\right] \tag{2.14}$$

With R_i from Eq. (2.2) $Y_{\lambda}^{(0)}(\theta_i)$ are the spherical harmonic function.

2.4.4 Rotational Energy due to angular momentum

The rotational motion gives an additional energy due to the angular momentum define as

$$V_l(R, A_i, \beta_{\lambda i}, \theta_i, T) = \hbar^2 \frac{l(l+1)}{2I_s(T)} \tag{2.15}$$

with $I(T) = I_{NS} = \mu R^2$, is the non-sticking limit of moment of inertia with as the $\mu = \frac{A_1 A_2}{A_1 + A_2} m$ reduced mass. m is the nucleon mass. In the complete sticking limit, the moment of inertia I is given as,

$$I_s(T) = \mu R^2 + \frac{2}{5} A_1 m R_1^2 + \frac{2}{5} A_2 m R_2^2 \tag{2.16}$$

with R_i from Eq. (2.2). However, for the relative separation of interest here, we use the sticking limit. It is relevant to mention here that value of angular momentum extracted experimentally, is based upon moment of inertia limit (i.e. ($I_{NS} = \mu R^2$)). It means that fragment emission is punctual. In our study, however, we find that sticking limit is more appropriate for the proximity potential which consequently results in much larger limiting value of angular momentum [26].

References

[1] R. K. Gupta, S. Kumar and W. Scheid 1995 *J. Phys. G: Nucl. Part. Phys.* 21 L27

[2] R. K. Gupta, M. Balasubramaniam , R. K. Puri and W. Scheid 2000 *J. Phys. G: Nucl. Part. Phys.* 26 L23

[3] J. Maruhn and W. Greiner, Phys. Rev. Lett. 32, 548 (1974).

[4] R. K. Gupta, W. Scheid and W. Greiner, Phys. Rev. Lett. 35, 353 (1975).

[5] A. Săndulescu, R.K. Gupta, W. Scheid and W. Greiner, Phys. Lett. 60B, 225 (1976).

[6] R. K. Gupta, A. Săndulescu and W. Greiner, Phys. Lett. 67B, 257 (1977); Rev. Roum. Phys. 23, 51 (1978).

[7] M. K. Sharma ,S. Kanwar, G. Sawhney, R. K. Gupta and W. Greiner, J. Phys. G: Nucl. Part. Phys. 38, 055104 (2011).

[8] S. K. Arun, R. K. Gupta, S. Kanwar, B. B. Singh and M. K. Sharma Phys. Rev. Lett. C 79, 064616 (2009)

[9] S. K. Arun, R. K. Gupta, S. Kanwar, B. B. Singh and M. K. Sharma Phys. Rev. Lett. C 80, 034317 (2009)

[10] R. K. Gupta, A. Săndulescu and W. Greiner, Z. Naturforsch. 32a, 704 (1977).

[11] R. K. Gupta, C. Pirvulescu, A. S¡andulescu and W. Greiner, Z. Phys. A 283, 217 (1977); Sovt. J. Nucl. Phys. 28, 160 (1978).

[12] R. K. Gupta, Z. Physik. A 281, 159 (1977).

[13] A. Săndulescu, H.J. Lustig, J. Hahn, and W. Greiner, J. Phys. G: Nucl. Phys.4, L279 (1978).

[14] H. J. Lustig, J.A. Maruhn, and W. Greiner, J. Phys. G: Nucl. Phys. 6, L25 (1980).

[15] H. J. Fink and W. Greiner and R.K. Gupta and S. Liran and J.H. Maruhn and W. Scheid and O. Zohni, in Proceedings of Int. Conf. on Reaction between Complex Nuclei, Nashville, 1974, 21, (Amsterdam: North Holland), pages 2.

[16] R. K. Gupta, IANCAS Bull. (India), 6, 2(1990).

[17] G. Sawhney, M. K. Sharma and R. K. Gupta Phys. Rev. C 83, 064610 (2011).

[18] W. Myers and W. J. Swiatecki 1966 *Nucl. Phys.* 81 1

[19] P.G. Hansen and B. Jonson 1987 *Europhys. Lett.* 4 409

[20] G. Audi and A.H. Wapstra and C. Thiboult, Nucl. Phys. A 729, 337(2003)

[21] P. M¨oller, J. R. Nix, W. D. Myers, and W. J. Swiatecki, At. Data Nucl. Data Tables 59, 185 (1995).

[22] V.M. Strutinsky, Nucl. Phys. A 95, 420 (1967).

[23] M. Balasubraniam, R. Kumar, R.K. Gupta, C. Beck, and W. Scheid, J. Phys. G 29, 2703 (2003):

[24] J. Blocki, J. Randrup, W. J. Swiatecki, and C. F. Tsang, Ann. Phys. (NY) 105, 427 (1977).

[25] Deryagin, Z. Kolloid 69, 155 (1934).

[26] B. B. Singh, M. K. Sharma and R. K. Gupta, Phys. Rev. C 77, 054613 (2008).

Chapter 3

3.1 Calculations and Discussion

We have studied the fragmentation path of some lighter nuclei near the neutron drip line and proton drip line. The nucleon rich nuclei near the drip lines i.e. neutron-rich (n-rich) or proton-rich (n-rich) light nuclei are totally unstable systems and hence show halo behaviour. In the present work we have done extensive calculations on neutron (n) halo nuclei. All halo nuclei are loosely bound due to weak binding of valance nucleons surrounding the core. The radius for such a nucleus have far more extended neutron density distribution (for n-halo) and extended proton density distribution (for p-halo) and are found to be much larger than that of expected radius from the formula $R = R_0A^{1/3}$. We have studied 1n- and 2n-halo nuclei with the help of Cluster Core Model (CCM) [1-2] extended to include the deformations and orientations of nuclei. In CCM, we calculate potential energy surfaces (PES) of a nucleus for its all possible cluster-core (A_2, A_1) configurations and look for the minimum value of potential energy surfaces (PES).

The cluster is neutron and proton in neutron halo nuclei and proton halo nuclei respectively. The neutron(s) cluster + core configurations corresponds to the minima in neutron(s) PES and is referred as n-halo nuclei whereas proton(s) cluster+ core configurations corresponds to the minima in proton(s) PES and is referred to p-halo nuclei. The minimum in PES means a most probable cluster + core configuration for the nucleus and the most probable configuration means that the cluster has the largest preformation probability in the language of Preformed Cluster Model (PCM). In this work we have done calculations for the spherical as well as for deformed configuration up to quadrupole deformations (β_2) considerations. Beside this an effort is also made to study the angular momentum effect on the halo nuclei. It has been seen that the deformation plays an important role for the nuclei with higher mass number (A). Although the halo nuclei under the present study are lighter in mass number yet deformations are supposed to play significant role because of large deformed shapes of these nuclei. Further the role of angular momentum also seems to affect the structure of the halo nuclei in some cases.

Table 3.1 The calculated 1n-halo characteristics of light neutron-rich nuclei. The neutron separation energies are calculated by using the binding energy table of [3] and configuration resulting from the PES (potential energy surfaces) are with respect to ℓ = 0,4ħ and 8ħ for spherical as well as for deformed nuclei.

Nucleus (1n-halo)	S_{1n}(KeV)	S_{2n}(KeV)	PES minimum (cluster+core configuration for spherical nuclei)	PES minimum (cluster+core configuration for deformed nuclei)
^{11}Be	556.4	7343.6	1n + ^{10}Be	1n + ^{10}Be
^{14}B	1019.7	5789.6	1n + ^{13}B	1n + ^{13}B
^{15}C	668.2	9207.8	1n + ^{14}C	1n + ^{14}C
^{17}C	789.8	5623.2	1n + ^{16}C	1n + ^{16}C
^{19}C	669.8	4526.3	1n + ^{18}C	1n + ^{18}C
^{22}N	507.8	4571.3	1n + ^{21}N	1n + ^{21}N
^{22}O	6170	9979.7	1n + ^{21}O	^{4}Li + ^{18}B
^{23}O	4006.6	10176.6	1n + ^{22}O	1n + ^{22}O
^{24}O	2751.1	6757.7	1n + ^{23}O	1n + ^{23}O
^{24}F	4460.4	11213.9	1n + ^{23}F	1n + ^{23}F
^{26}F	-390	4651.2	1n + ^{25}F	1n + ^{25}F
^{29}Ne	2983.3	7443.5	1n + ^{28}Ne	1n + ^{28}Ne
^{31}Ne	330	3300	1n + ^{30}Ne	^{14}Be + ^{17}C

We have calculated the PES for 13 cases of 1n-halo nuclei which includes ^{11}Be, ^{14}B, ^{15}C, ^{17}C, ^{19}C, ^{22}N, ^{22}O, ^{23}O, ^{24}O, ^{24}F, ^{26}F,^{29}Ne and ^{31}Ne listed in table 3.1 and 11 cases of 2n-halo nuclei which will be discussed after the discussion of 1n-halo nuclei. The fragmentation potential used for a cluster–core configuration (A_2, A_1) of a nucleus A is defined as sum of binding energies, Coulomb repulsion, additional attraction due to nuclear proximity and rotational energy due to angular momentum as already discussed in model (chapter 2). Also neutron separation energy hypothesis is another method to derive the halo structure of a neutron or proton rich light nuclei. The neutron separation energy are listed in table 3.1 for all 1n-halo nuclei which are calculated in terms of binding energy *B (Z, N)* as

$$S_{1n} = M\,(Z, N\text{-}1) + M_n - M\,(Z, N) = B\,(Z, N) - B\,(Z, N\text{-}1)$$

and
$$S_{2n} = M\,(Z, N\text{-}2) + M_{2n} - M\,(Z, N) = B\,(Z, N) - B\,(Z, N\text{-}2) \qquad (3.1)$$

for the 1n and 2n halo nuclei respectively. Similarly for proton halo nuclei the separation energies are calculated as

$$S_{1p} = M(Z\text{-}1, N) + M_p - M(Z, N) = B(Z, N) - B(Z\text{-}1, N)$$

$$S_{2p} = M(Z\text{-}2, N) + M_{2p} - M(Z, N) = B(Z, N) - B(Z\text{-}2, N) \quad (3.2)$$

for 1p and 2p-halo nuclei. According to separation energy method for halo structure, the 1n and 2n separation energies should be lowest and less than 1 MeV (to be compared with 6-8 MeV for stable nuclei). A nucleus is said to be 1n or 2n- halo if S_{1n} or S_{2n} is lowest or less than 1MeV. Table 3.1 clearly shows that PES minimum comes at 1n for the chosed halos, irrespective of the choice of deformation except for ^{22}O, which has been discussed later in Fig. 3.6.

3.1.1 ONE NEUTRON (1n) HALO NUCLEI

We have calculated potential energy surfaces for a large no. of neutron rich nuclei with and without incorporating nuclear deformation effects. The inclusion of deformation effects impart some important information in reference to the structure of halo nuclei. All these calculations are done for the ground state decay of nuclei i.e. at temperature T=0.

(1) Firstly, Fig. 3.1 shows the fragmentation potential plotted as the function of fragment mass no. at different ℓ values for ^{11}Be nuclei. The fragmentation path is shown for spherical, deformed (hot) as well as deformed (cold) configurations. It is evident from the Fig.3.1 that the structure of PES in spherical nuclei remains same at lower ℓ values i.e. at ℓ = 0 and 4ħ but there is a significant change in structure of PES as one goes to higher ℓ value i.e. at ℓ=8 ħ.

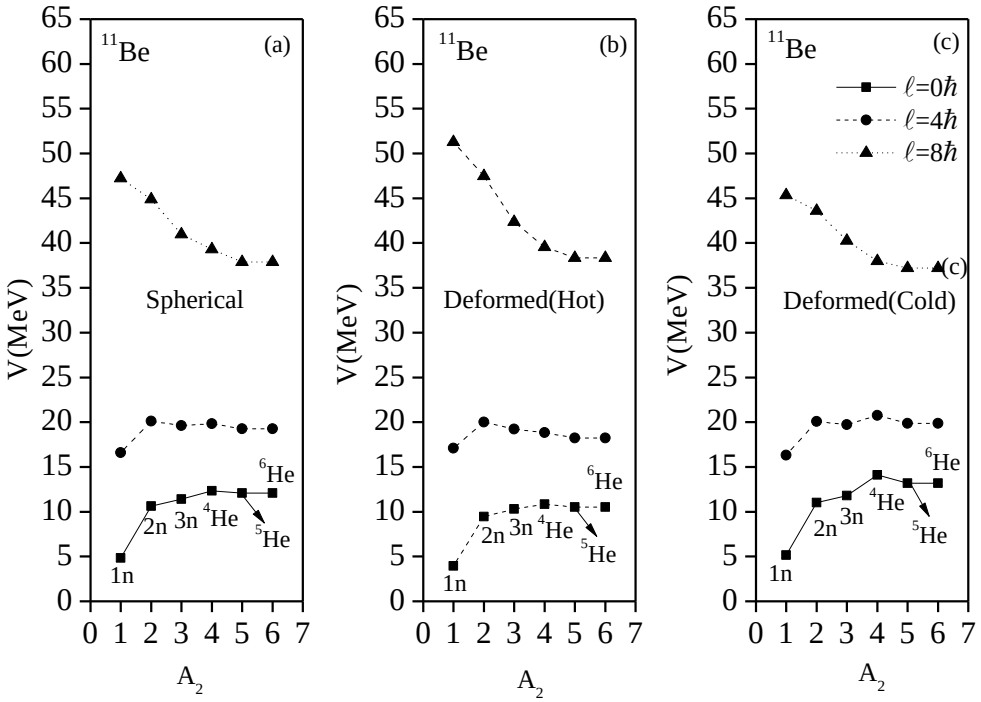

Fig. 3.1

It is clearly evident from the fig. that the deepest minimum in potential energy surfaces (PES) occurs 1n + core configuration for spherical nuclei (Fig.3.1 (a)) at lower value of angular momentum but for the higher angular momentum $\ell = 8\ \hbar$ (say), the minimum value of PES V (A_2) does not remain same i.e. the minima shifts to another cluster at higher angular momentum for spherical case. It means that structure of PES changes significantly at higher angular momentum ℓ values which indicates that the role of angular momentum needs to be dealt with care in reference to light nuclear systems. However one can see that there is no significant change in the potential energy surfaces (PES) behaviour as one goes from spherical to deformed case for higher as well as lower ℓ (shown in Fig. 3.1(a) and (b)). This means that the deformations are not playing any significant role in case of ^{11}Be nuclei. Further in order to draw comparison between hot and cold orientation, one can compare the PES behaviour (Fig. 3.1(b) and (c) for the decay of ^{11}Be. The "hot compact" configurations corresponds to smallest interaction radius and highest barrier whereas the "cold non compact" configurations correspond to large interaction radius and lowest barrier. Again there is no significant change in the structure of fragmentation potential as one goes from hot to cold configuration. In reference to this observation we have done all the calculations only for the optimally oriented hot configuration.

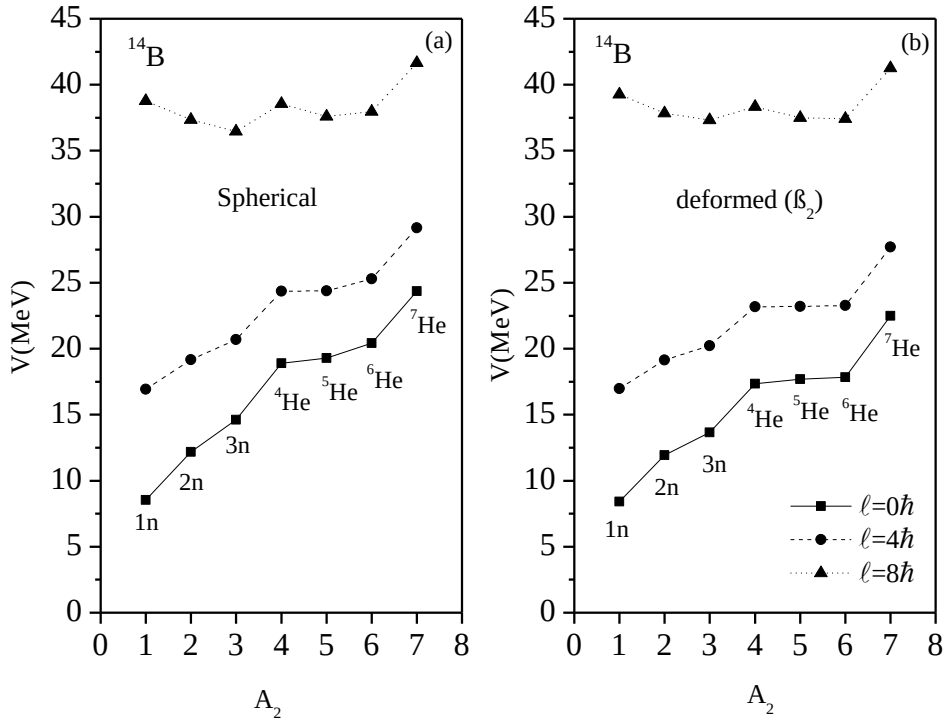

Fig. 3.2

(2) Secondly, it has been seen that for various nuclei like ^{14}B, ^{17}C, ^{19}C and ^{22}N the structure changes as one goes from spherical to deformed nuclei at higher value of angular momentum i.e. at ℓ = 8 ħ. Figs. 3.2, 3.3, 3.4 and 3.5 shows PES behaviour for ^{14}B, ^{17}C, ^{19}C and ^{22}N nuclei. Interestingly, the minima in all nuclei occur at 1n+core configuration whereas the minima shifts to 3n+core configuration for ℓ = 8 ħ i.e. at higher angular momentum for the spherical as well as deformed consideration.

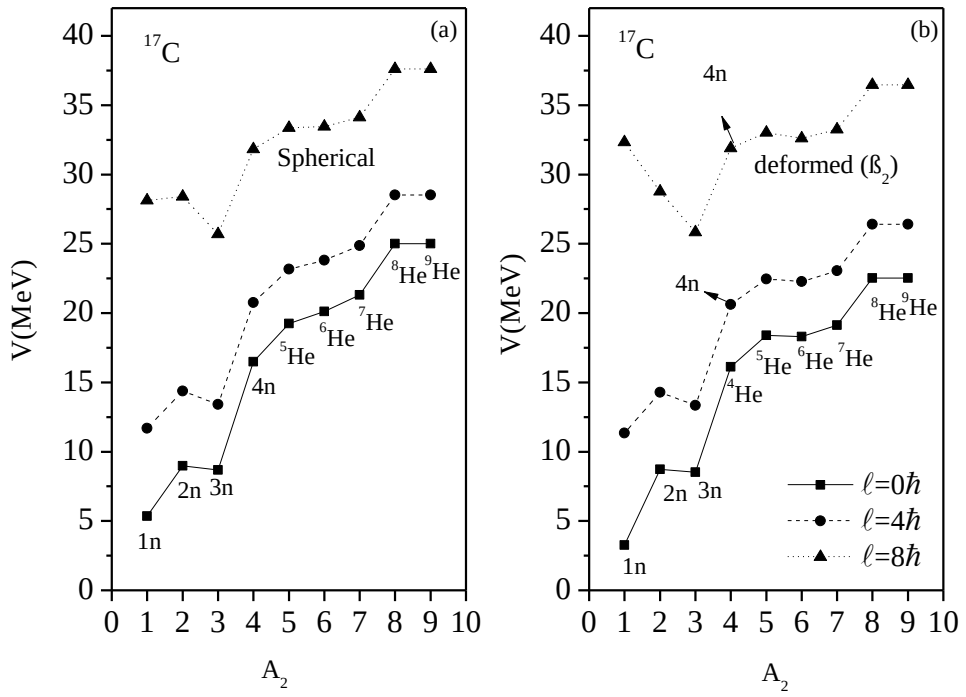
(a)
^{17}C
Spherical
1n
2n
3n
4n
^{5}He
^{6}He
^{7}He
^{8}He
^{9}He
V(MeV)
A$_2$
(b)
^{17}C
deformed (ß$_2$)
4n
^{4}He
ℓ=0ħ
ℓ=4ħ
ℓ=8ħ

Fig. 3.3

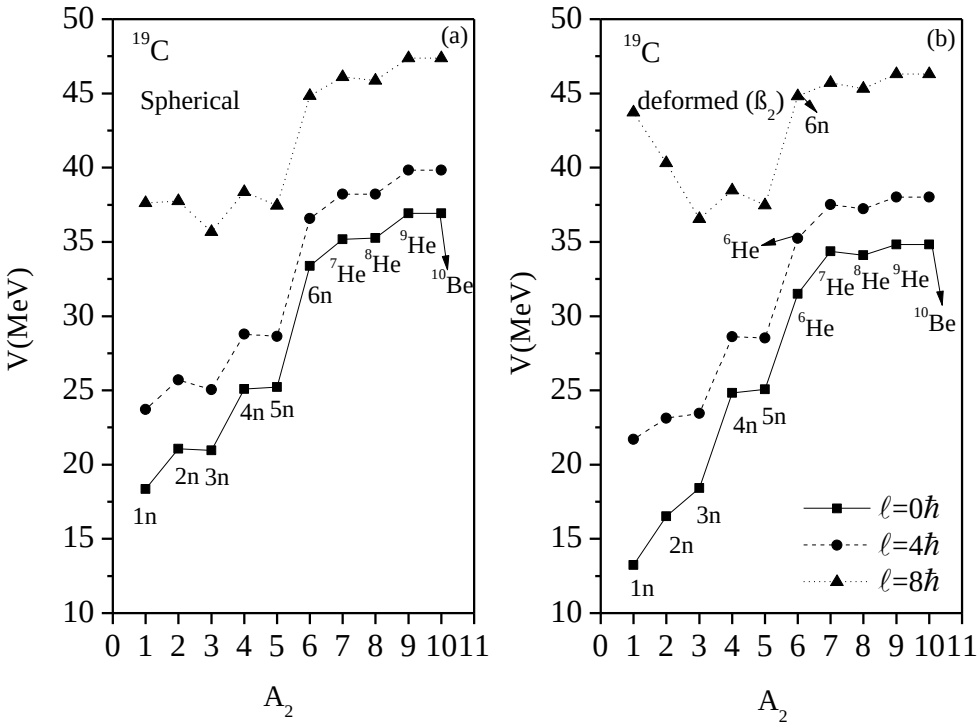
(a)
^{19}C
Spherical
1n
2n
3n
4n
5n
6n
^{7}He
^{8}He
^{9}He
^{10}Be
V(MeV)
A$_2$
(b)
^{19}C
deformed (ß$_2$)
^{6}He
^{7}He
^{8}He
^{9}He
^{10}Be
ℓ=0ħ
ℓ=4ħ
ℓ=8ħ

Fig. 3.4

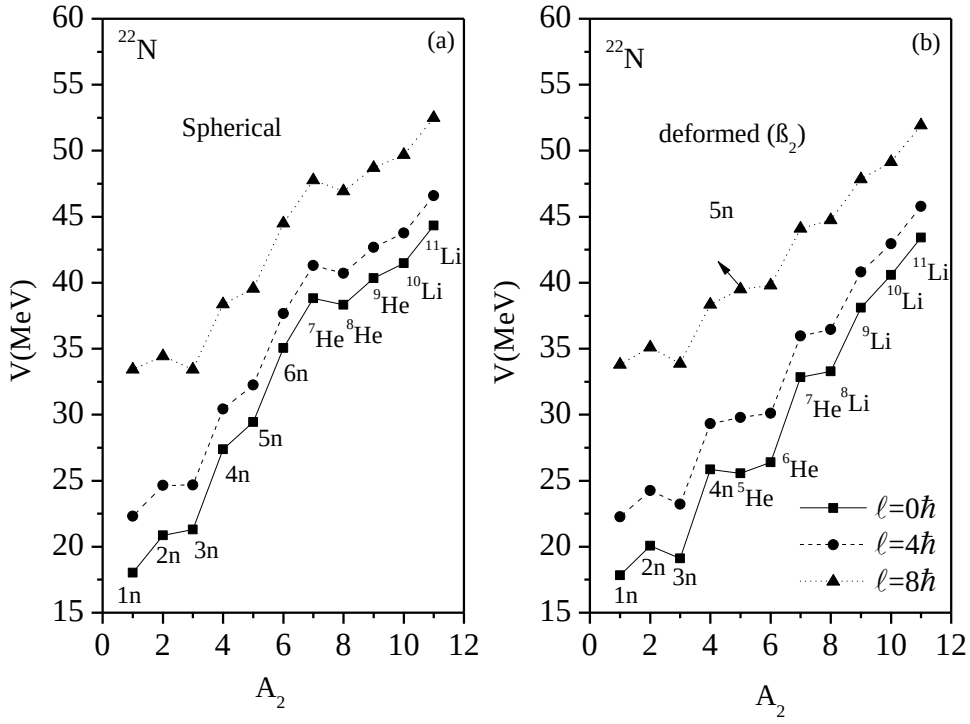

Fig. 3.5

Also structure of PES for ^{22}N nuclei in Fig. 3.5 shows that the fragments corresponding to the minima in PES do not remain same as one go from spherical to deformed nuclei at higher mass number for ℓ = 0ħ. The minima of PES at 5n and 6n Fig. 3.5 (a) for spherical case changes to ^{5}He and ^{6}He for deformed nuclei in Fig. 3.5 (b) at ℓ = 0ħ. Similarly the minima at the fragments ^{8}He and ^{9}He for spherical case change to ^{8}Li and ^{9}Li for deformed case at lower value of angular momentum. In addition, ^{22}N nuclei has the highest mass number in comparison to other nuclei like ^{14}B, ^{17}C and ^{19}C which signifies that for neutron rich halo nuclei deformation effects are more sensitive.

(3) Interestingly for ^{22}O, the minima of potential energy surfaces (PES) changes when we go from spherical to deformed nuclei even at zero angular momentum ℓ = 0ħ. Fig. 3.6 shows that ^{22}O nuclei has different minima's corresponding to PES for both spherical and deformed nuclei even at ℓ = 0ħ. This is an exceptional case from all the 1n- halo nuclei listed in table 3.1. In spherical nuclei, the minima in PES occurs at 1n+core configuration however it shifts to ^{4}Li+core configuration when we move from spherical to deformed nuclei. However, the most preferred cluster-core configuration at all ℓ values in the decay of ^{22}O is 1n+core.

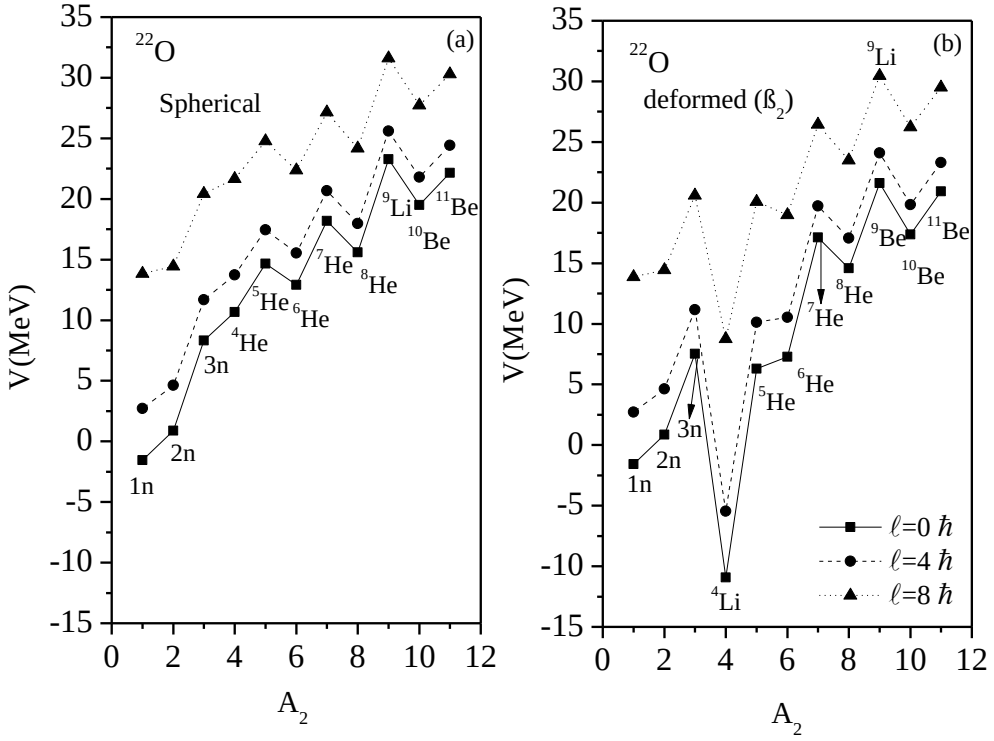

Fig. 3.6

(4) Fourthly, it has been seen that the structure of the potential energy surfaces changes significantly with inclusion of deformations and orientations at lower angular momentum i.e. ℓ = 0ħ for ^{23}O, ^{24}O, ^{26}F and ^{29}Ne nuclei as shown in Figs. 3.7, 3.8, 3.9 and 3.10. Thus the deformations and orientations of decaying nuclei plays significant role even at ℓ = 0ħ for ^{23}O, ^{24}O, ^{26}F and ^{29}Ne halo systems. However 1n-halo structure remains intact irrespective of spherical or deformed configuration.

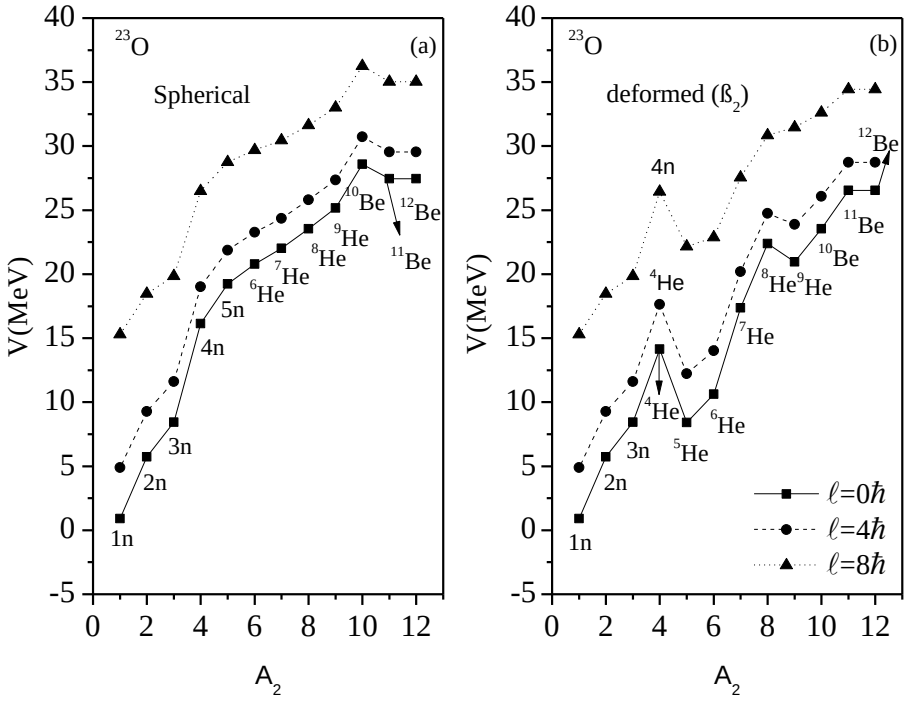
(a)
^{23}O
Spherical
V(MeV)
A$_2$
1n
2n
3n
4n
5n
^{6}He
^{7}He
^{8}He
^{9}He
^{10}Be
^{11}Be
^{12}Be
(b)
^{23}O
deformed (ß$_2$)
^{4}He
^{5}He
ℓ=0$\hbar$
ℓ=4$\hbar$
ℓ=8$\hbar$

Fig. 3.7

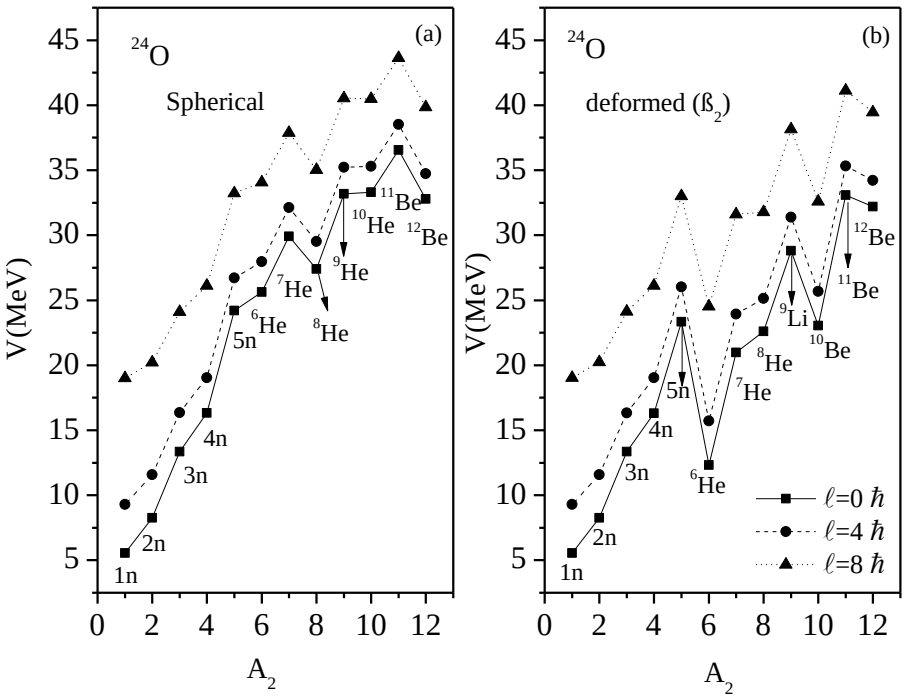
(a)
^{24}O
Spherical
V(MeV)
A$_2$
1n
2n
3n
4n
5n
^{6}He
^{7}He
^{8}He
^{9}He
^{10}He
^{11}Be
^{12}Be
(b)
^{24}O
deformed (ß$_2$)
^{9}Li
^{10}Be
ℓ=0 $\hbar$
ℓ=4 $\hbar$
ℓ=8 $\hbar$

Fig. 3.8

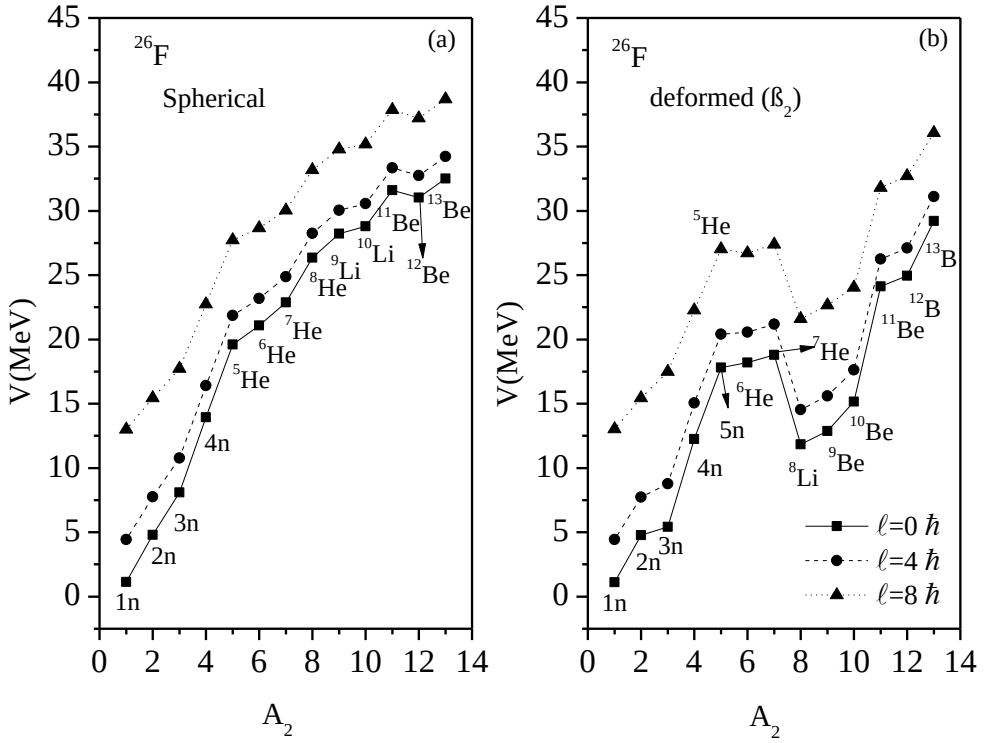

Fig. 3.9

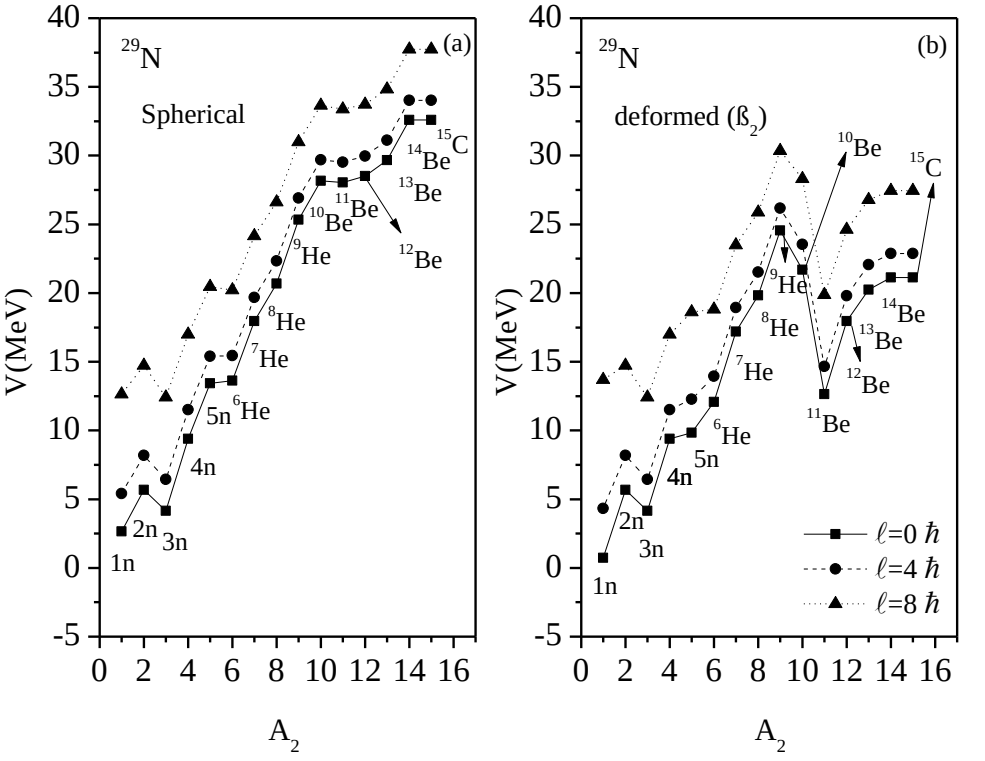

Fig. 3.10

(5) Lastly, the nuclei ^{15}C and ^{24}F are of the particular interest from all the above 1n-halo nuclei. The structure for this nuclei remains same for lower angular momentum i.e. at $\ell = 0$ and $4\hbar$ as well as for higher angular momentum i.e. at $\ell = 8\hbar$. The deformations do not seem to effect much in these nuclei. One can clearly see from Figs. 3.11 and 3.12 that with the inclusion of deformation and orientation the structure of PES remain intact while going from spherical to deformed considerations. Along with the structure of PES, the minima in both these nuclei are shown to occur at 1n+core configuration for both spherical and deformed cases.

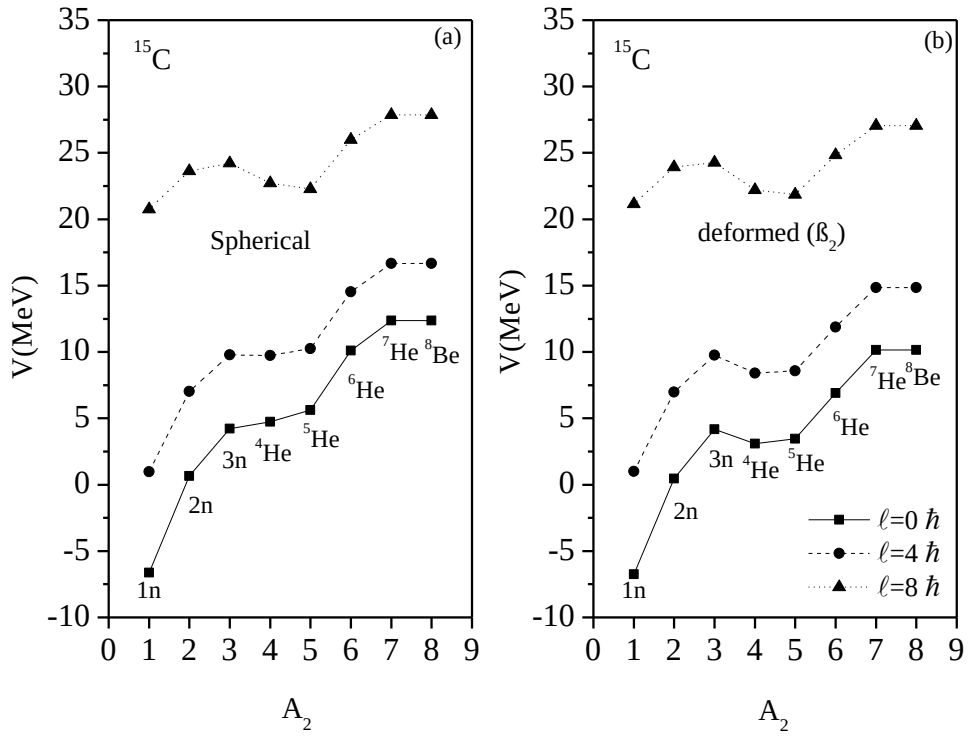

Fig. 3.11

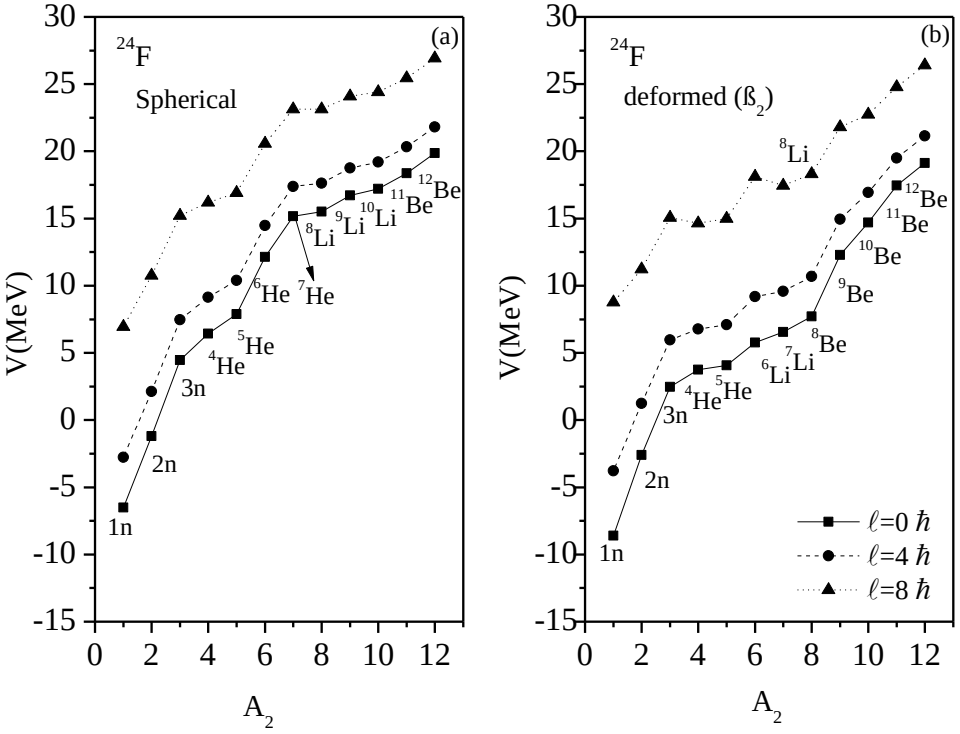

Fig. 3.12

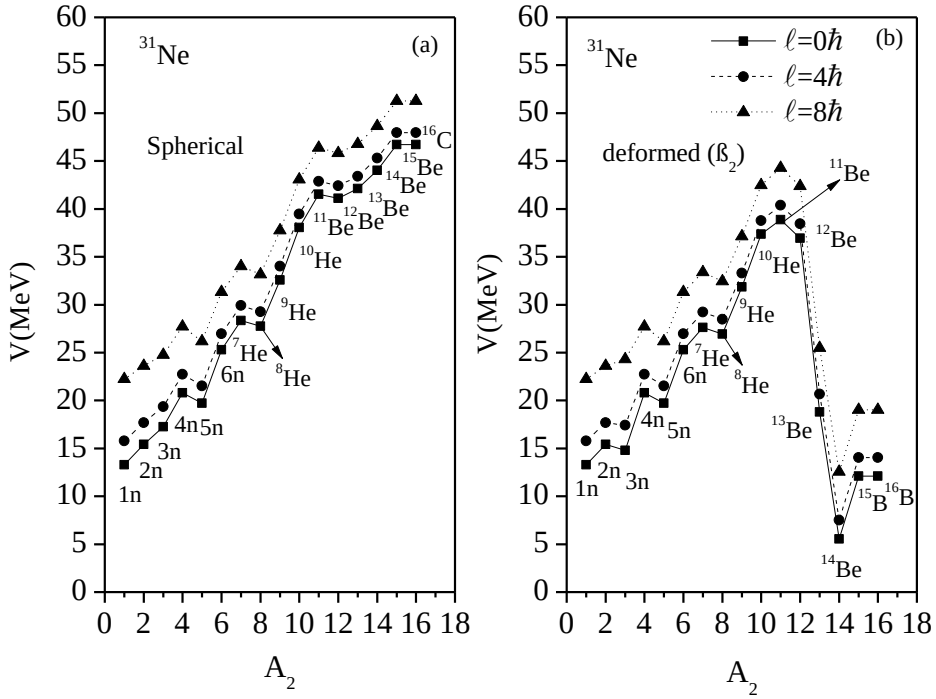

Fig. 3.13

The ^{31}Ne nucleus has been investigated in recent times [4, 5, 6]. We have studied the deformation and angular momentum effects on this nucleus using CCM in order to have further understanding of its nuclear structure and halo status. The minimum in potential energies surfaces for the ^{31}Ne nucleus with and without deformation effects are shown in Fig.3.13. This nucleus gives 1n-halo structure for $\ell = 0$ to $\ell = 8\hbar$ for ground state decay i.e. at T = 0 for spherical as well as deformed configuration of fragmentation. In other words the most preferred cluster+core configuration for this decay of nucleus is 1n+core configuration for spherical as well as for deformed case in agreement with [4]. However, the minima in PES show reversal in behaviour for heavier fragments with inclusion of deformation and orientation effects. As the data for 1n removal cross-section and interaction cross-section [5, 6] is available so it will be of further interest to test this data with CCM approach.

Further we have calculated the 1n and 2n separation energy (S_{1n} and S_{2n}) by using formula as given by equation (3.1) for all the 1n-halo nuclei listed in table 1. The separation energies (S_{1n}) for ^{11}Be, ^{14}B, ^{15}C, ^{17}C, ^{19}C, ^{22}N and ^{31}Ne 1n-halo nuclei are found to be less than or near to 1MeV. The notable exceptions from all the 1n-halo nuclei listed in table 3.1 are ^{22}O, ^{23}O, ^{24}O, ^{24}F, ^{26}F and ^{29}Ne nuclei. In all these cases one neutron separation energy (i.e. S_{1n}-value) is greater than 1MeV whereas in all these cases except ^{22}O the minima in the PES lies at 1n+core configuration.

3.1.2 TWO NEUTRON (2n) HALO NUCLEI

We have calculated the potential energy surfaces (PES) for 11 cases of 2n-halo nuclei which includes ^{6}He, ^{8}He, ^{11}Li, ^{12}Be, ^{14}Be, ^{17}B, ^{19}B, ^{22}C, ^{23}N, ^{27}F and ^{29}F listed in table 3.2. All these nuclei give 2n-halo structure for spherical as well as deformed case except for the ^{17}B and ^{22}C. For ^{17}B and ^{22}C the minima in PES shifts to 1n+core configuration and 4n+core configuration with the inclusion of deformation and orientation effects at $\ell = 0\hbar$ giving rise to 1n and 4n halo structure for ^{17}B and ^{22}C nuclei.

Similar to 1n-halo cases the deformations as well as angular momentum seem to play an significant role in ground state decay of 2n-halo nuclei as well. The explanation is discussed below for these 2n-halo nuclei.

Table 3.2 The calculated 2n-halo characteristics of light neutron-rich nuclei. The neutron separation energies are calculated by using the binding energy table of [3] and configuration resulting from the PES (potential energy surfaces) are with respect to ℓ = 0,4ħ and 8ħ for spherical as well as for deformed nuclei.

Nucleus (2n-halo)	S_1(KeV)	S_{2n}(KeV)	PES minimum (cluster+core configuration for spherical nuclei)	PES minimum (cluster+coreconfiguration for deformed nuclei)
^{6}He	1966.3	1120	2n + ^{4}He	2n + ^{6}He
^{8}He	2957.9	2072.8	2n + ^{6}He	2n + ^{4}He
^{11}Li	355	323.7	2n + ^{9}Li	2n + ^{9}Li
^{12}Be	3227.4	3783.8	2n + ^{10}Be	2n + ^{10}Be
^{14}Be	1857.7	1351.1	2n + ^{12}Be	2n + ^{12}Be
^{17}B	1480.7	1431.6	2n + ^{15}B	1n + ^{16}B
^{19}B	955	438.6	2n + ^{17}B	2n + ^{17}B
^{22}C	2471	1925.3	2n + ^{20}C	4n + ^{18}C
^{23}N	8071.0	16142	2n + ^{21}N	2n + ^{21}N
^{27}F	2015.4	1625.4	2n + ^{25}F	2n + ^{25}F
^{29}F	1978.2	875.7	4n + ^{25}F	2n + ^{27}F

Figs. 3.14, 3.15, 3.16, 3.17, 3.18 and 3.19 shows the fragmentation potential plotted for ^{6}He, ^{8}He, ^{11}Li, ^{12}Be, ^{14}Be and ^{19}B nuclei as a function of mass number. The structure for all these 2n-halo nuclei remains almost consistent when we include the effect of deformations (β_2) and orientations at both lower as well as higher ℓ values except for few cases like ^{14}Be and ^{19}B nuclei where the structure of potential energy surfaces changes significantly at higher ℓ value i.e. at ℓ = 8ħ as one goes from spherical to deformed case. Further in addition to role of deformations in 2n-halo nuclei, the angular momentum also seems to contribute significantly. For e.g. the minima in PES for ^{12}Be nuclei shifts to 4n+core configuration at higher ℓ value (ℓ = 8ħ) both for the spherical and deformed cases. In addition to this the 2n minima in PES for ^{14}B changes to 4n for spherical case and 5n for deformed case. Similarly in case of ^{19}B nuclei the minima of PES shifts to the 4n for higher ℓ values in spherical as well as in deformed case. Hence, the angular momentum effects are playing significant role in 2n-halo nuclei just like 1n-halo nuclei.

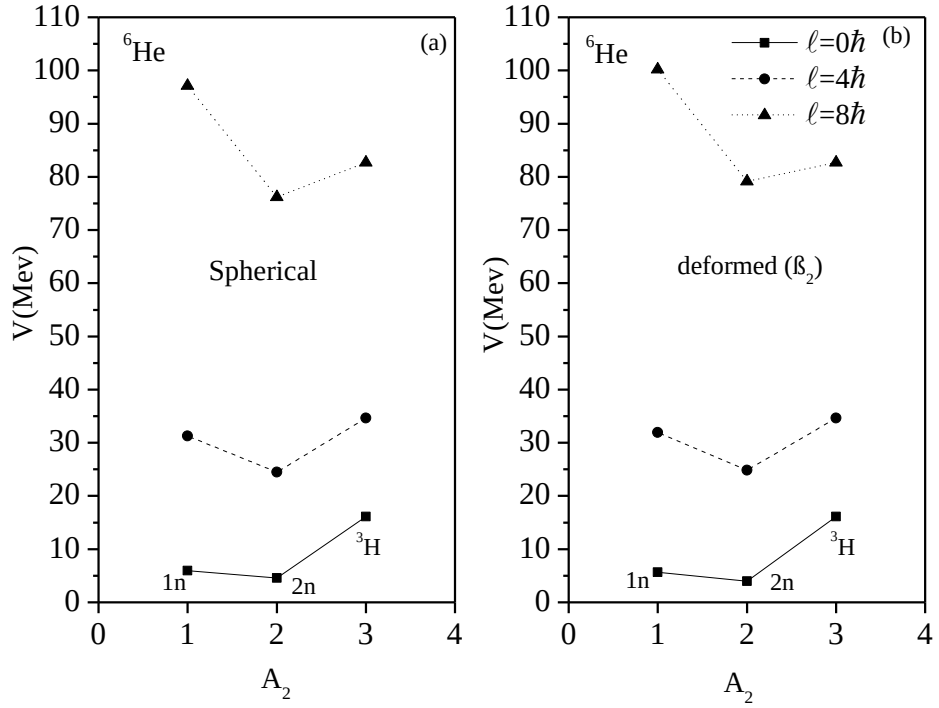

Fig. 3.14

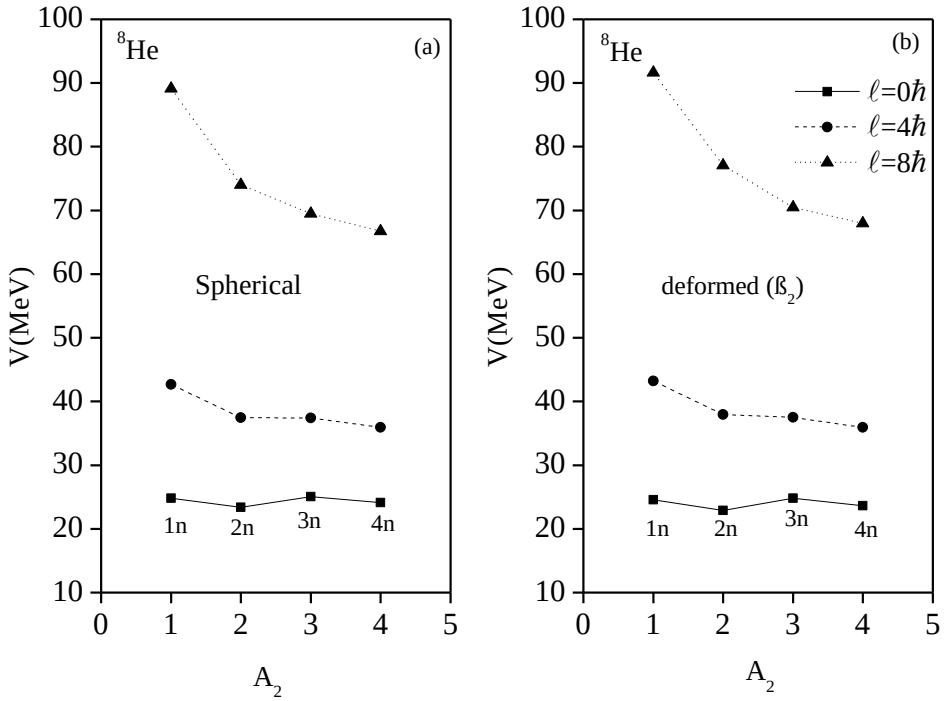

Fig. 3.15

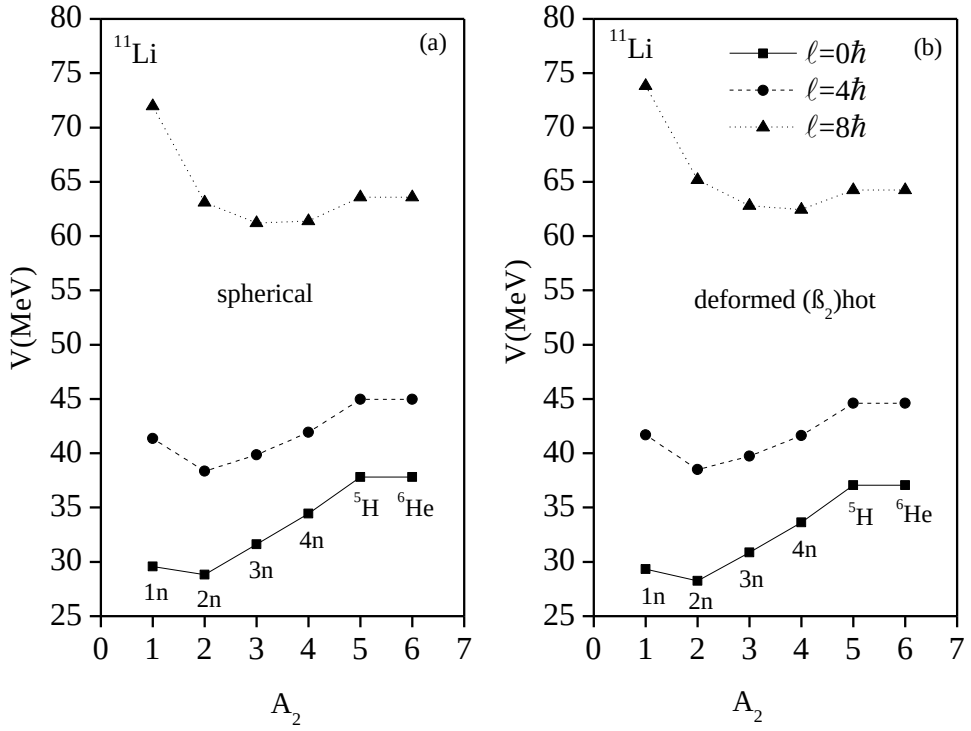

Fig. 3.16

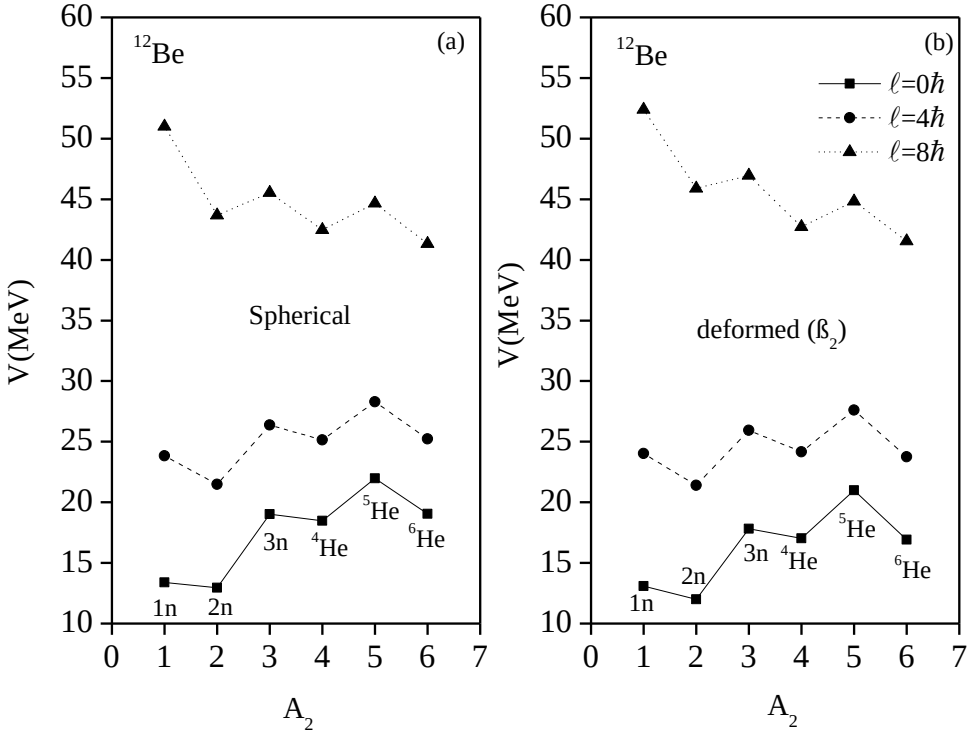

Fig. 3.17

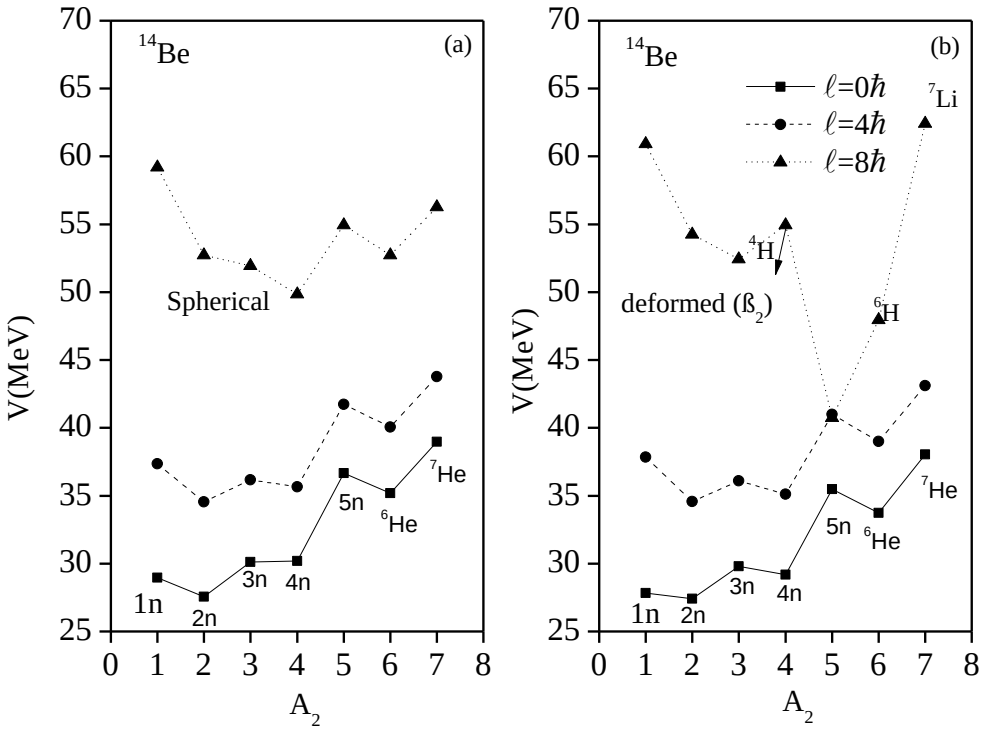

Fig. 3.18

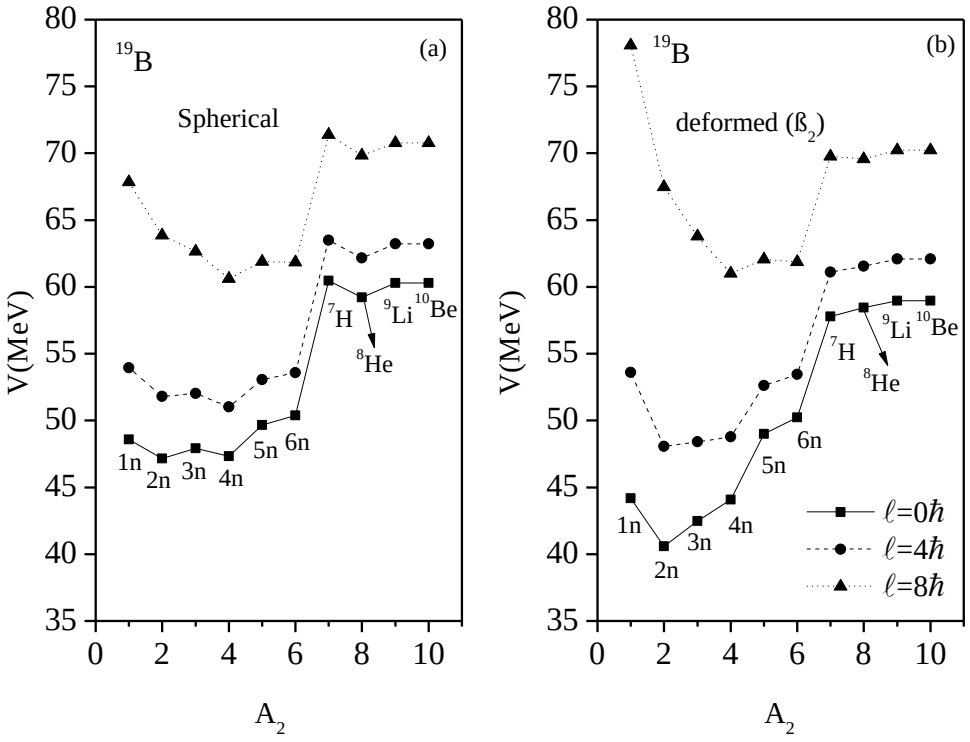

Fig. 3.19

Further the study of ^{17}B, ^{22}C, ^{23}N, ^{27}F and ^{29}F nuclei is of much interest because there is a significant change in the structure at $\ell = 0\hbar$ as one goes from spherical to deformed case. In addition to $\ell = 0\hbar$ case, the structure of fragmentation potential changes significantly at higher ℓ values i.e. at $\ell = 8\hbar$ for the cases of ^{23}N, ^{27}F and ^{29}F with the inclusion of deformation and orientation effects.

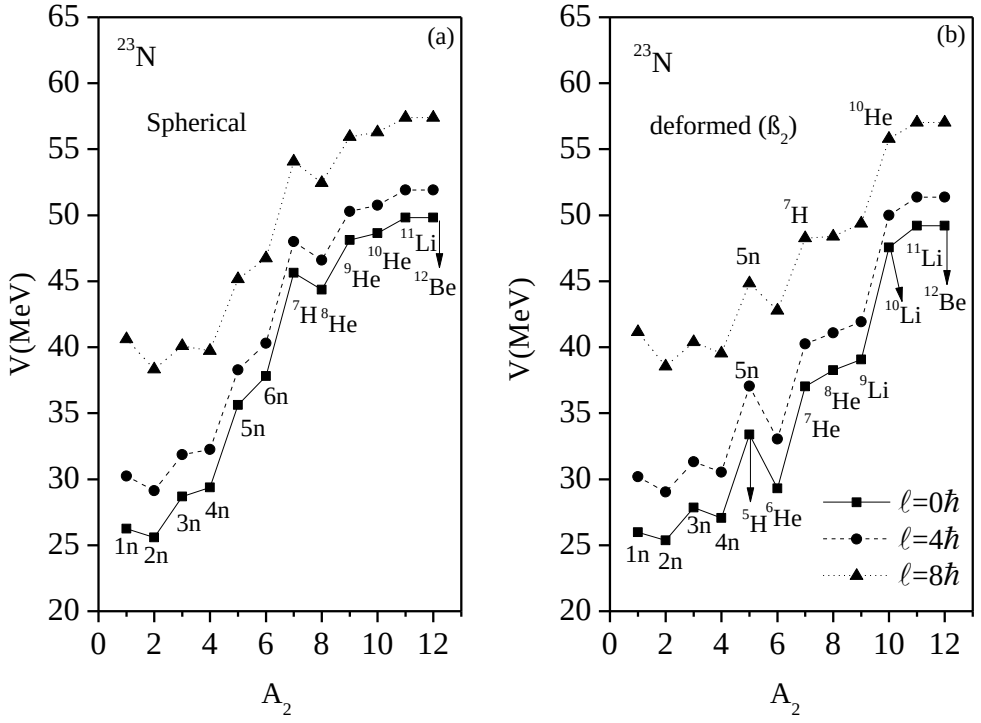

Fig. 3.20

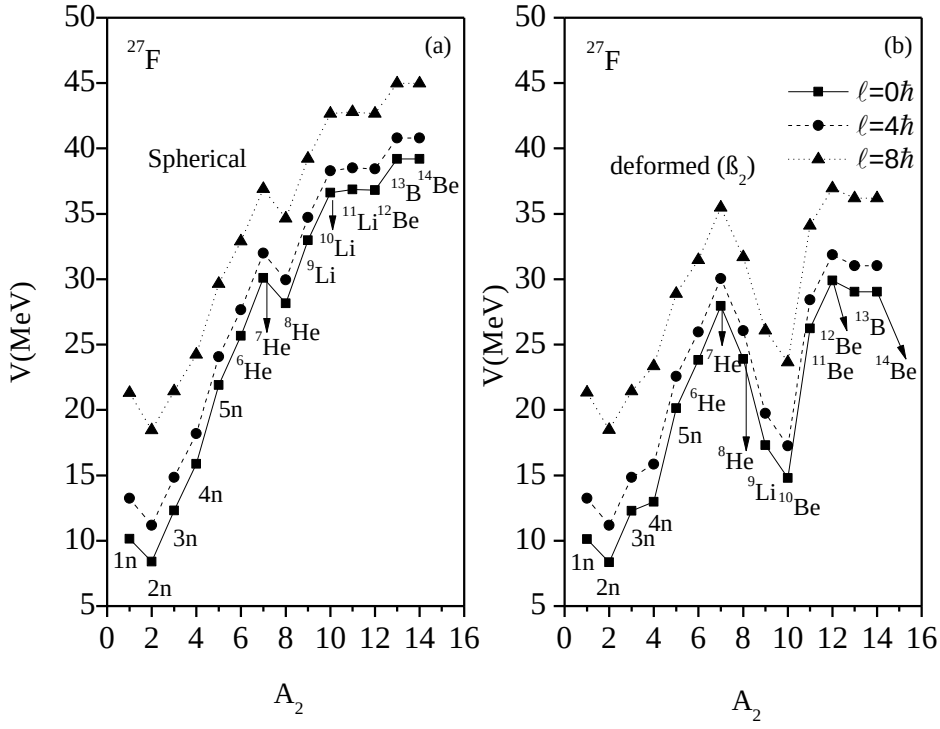

Fig. 3.21

Figs. 3.22, 3.23 and 3.24 show the behaviour of PES for ^{17}B, ^{22}C and ^{29}F nuclei. These are three most interesting nuclei among all the 2n-halo nuclei studied. In these halo nuclei the cluster + core configuration at ℓ = 0ħ changes after the inclusion of deformation and orientation effects. The minima of PES in case of ^{17}B and ^{22}C nuclei are at 2n+core configuration for spherical case but it shifts to 1n+core configuration for ^{17}B nuclei and 4n+core configuration for ^{22}C nuclei with inclusion of deformations and orientation effects. Interestingly, ^{29}F nuclei is of further interest as it shows its minima in PES at 4n+core configuration for spherical nuclei and it shifts to 2n+core configuration when deformation and orientation effects are added i.e. it gives 2n halo nuclei for deformed case whereas 4n-nuclei halo for spherical case. Thus ^{29}F nuclei shows an interesting result which can further be investigated to know more about the structure of the 2n-halo nuclei in the ground state decay of this nucleus.

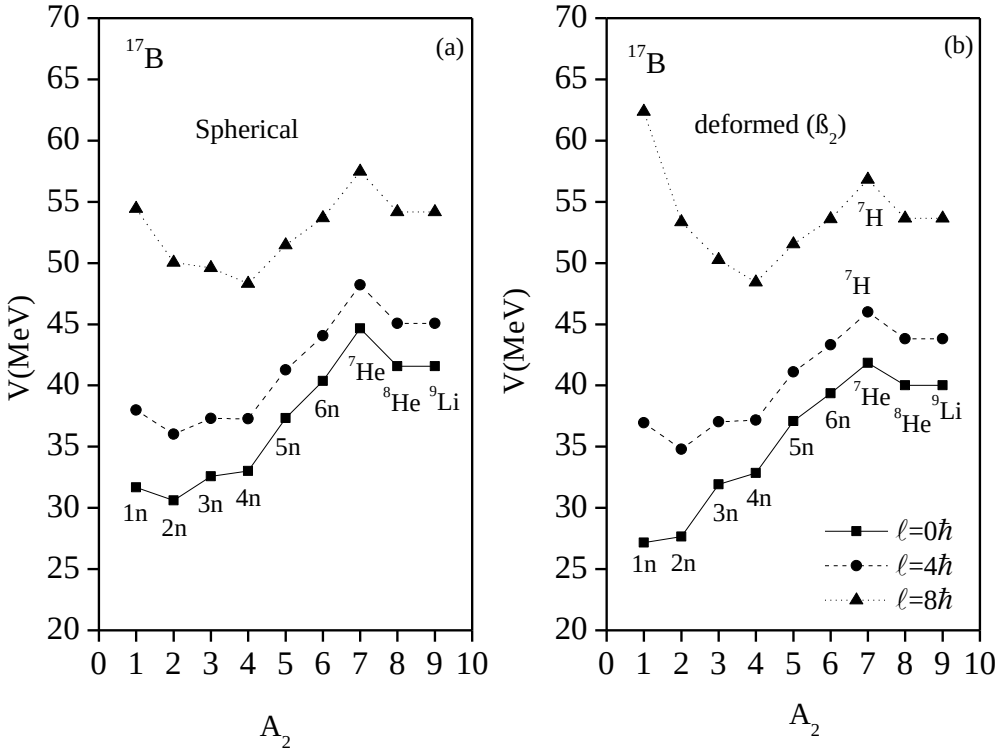

Fig. 3.22

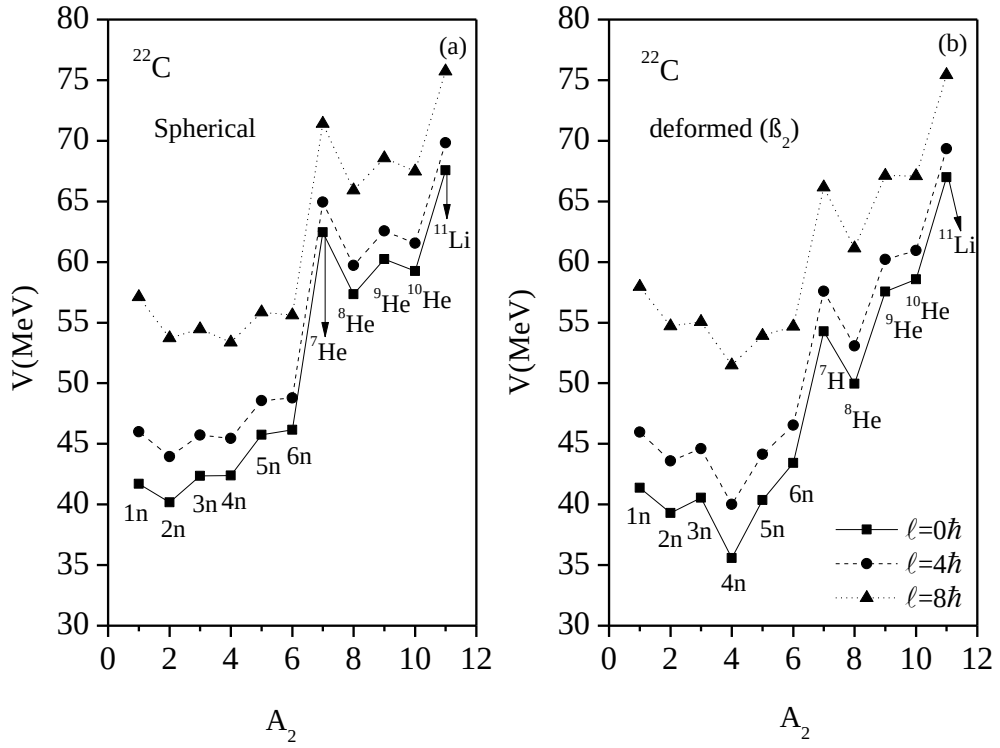

Fig. 3.23

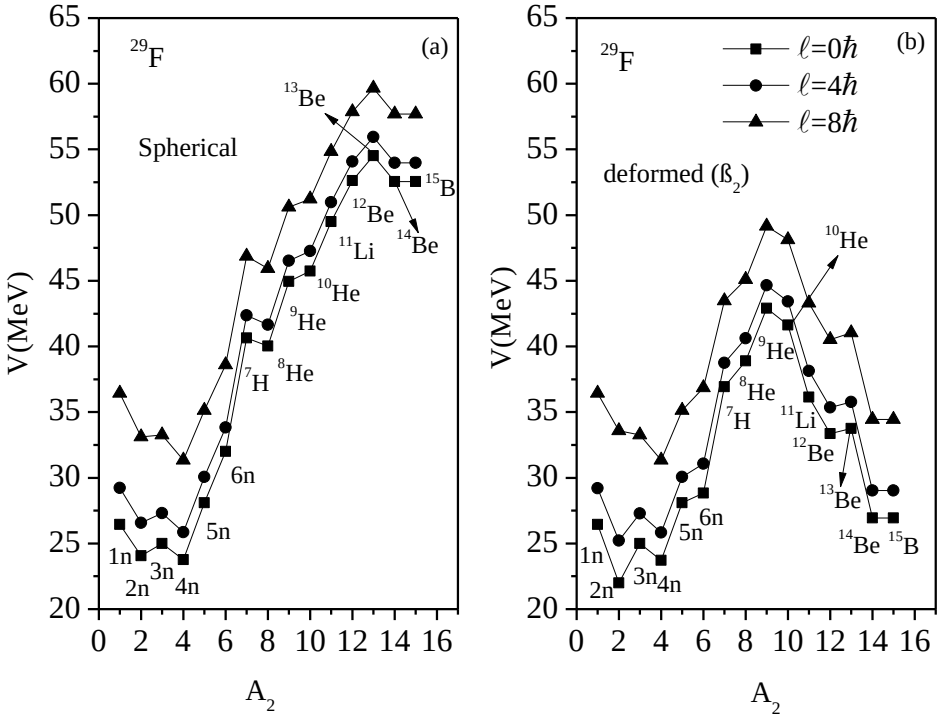

Fig. 3.24

Here also we have calculated the separation energies S_{1n} and S_{2n} by using same formula from equation (3.1) for all the 2n-halo nuclei. The S_{1n} or S_{2n} separation energies for ^{6}He, ^{8}He, ^{14}Be, ^{22}C, ^{27}F and ^{29}F, 2n-halo nuclei are found to be much larger than 1MeV. The notable exceptions from all the 2n-halo nuclei listed in table 2 are ^{12}Be and ^{23}N nuclei. In these two nuclei the S_{1n}-value is less than S_{2n}-value, whereas minimum in PES is clearly at 2n+core configuration for both spherical and deformed nuclei.

Magic number

In nuclear physics, a magic number is a number of nucleons (either protons or neutrons) such that they corresponds to complete shell within the atomic nucleus. The seven recognised magic numbers are Z = N = 2, 8, 20, 28, 50, 82 and N = 126. However Z = 114 or 120 or 126 and N = 178 or 184 are also being worked out in reference to super heavy region. Atomic nuclei consisting of such a magic number of nucleons have a higher average binding energy per nucleon than that of the predicted on the basis of semi-empirical mass formula and are hence more stable against nuclear decay.

Nuclei which have neutron number and proton (atomic) numbers each equal to one of the magic numbers are called "double magic", and are especially stable against decay. Examples of double magic isotopes include Helium-4 (^{4}He), Oxygen-16 (^{16}O), Calcium-40 (^{40}Ca), Calcium-48 (^{48}Ca), Nickel-48 (^{48}Ni) and Lead-208 (^{208}Pb)

Table 3.3 Possible Magic character of the core nucleus of some observed and theoretically possible 1n- halo nuclei.

Nucleus (1n-halo)	Cluster	Core (Spherical / Deformed)	Z (Spherical Deformed)	N (Spherical/ Deformed)	Possible Magic No.
^{11}Be	1n	^{10}Be	4	6	N = 6
^{14}B	1n	^{13}B	5	8	N = 8
^{15}C	1n	^{14}C	6	8	N = 8 ; Z= 6
^{17}C	1n	^{16}C	6	10	Z = 6
^{19}C	1n	^{18}C	6	12	Z = 6
^{22}N	1n	^{21}N	7	14	N = 14
^{22}O	1n / ^{4}Li	^{21}O / ^{18}B	8 / 5	13/ 13	Z = 8
^{23}O	1n	^{22}O	8	14	Z = 8
^{24}O	1n	^{23}O	8	15	Z = 8
^{24}F	1n	^{23}F	9	14	N = 14
^{26}F	1n	^{25}F	9	16	N = 16
^{29}Ne	1n	^{28}Ne	10	18	N = 18
^{31}Ne	1n	^{29}Ne	10	20	N = 20

Table 3.4 Possible Magic character of the core nucleus of some observed and theoretically possible 2 n- halo nuclei.

Nucleus (2n-halo)	Cluster	Core (Spherical / Deformed)	Z (Spherical/Deformed)	N (Spherical/Deformed)	Possible Magic No.
^{6}He	2n	^{4}He	2	2	N = Z = 2
^{8}He	2n	^{6}He	2	4	Z = 2
^{11}Li	2n	^{9}Li	3	6	N = 6
^{12}Be	2n	^{10}Be	4	6	N = 6
^{14}Be	2n	^{12}Be	4	8	N = 8
^{17}B	1n / 2n	^{16}B/ ^{15}B	5	11 / 10	-
^{19}B	2n	^{17}B	5	12	-
^{22}C	2n / 4n	^{20}C / ^{18}C	6	14 / 12	N=14, Z= 6
^{23}N	2n	^{21}N	7	14	N = 14
^{27}F	2n	^{25}F	9	16	N = 16
^{29}F	4n/2n	**^{25}F /** ^{27}F	9	16/18	N = 16,18

In the present work the ground state decay of nucleus give cluster+ core configuration. The minima in PES referred to most probable configuration as discussed earlier. The most probable configuration means most stable configuration as compared to other cluster+core configurations. We have seen that the core configuration changes for the ^{22}O in case of 1n-halo nuclei and ^{17}B, ^{22}C and ^{29}F in case of 2n-halo nuclei with the inclusion of deformation effects. The proton and neutron number for the most preferred configuration in table 3.3 and 3.4 are N or Z = 6 ,14, 16 so called new magic numbers in language of halo nuclei, along with well known magic number N = Z = 8. As stated earlier, the core configuration changes for ^{22}O (1n-halo) and ^{17}B, ^{22}C, and ^{29}F (2n-halo) nuclei with the inclusion of deformation and orientation effects. Which in other words suggest a new cluster core configuration in halo region. However the present observations are made only on the basis of fragmentation potential, so further efforts are required to meet definite conclusion.

Summary

The above whole discussion indicates that the role of deformation and orientations along with angular momentum is important for neutron halo nuclei. In summary angular momentum at $\ell > 4\hbar$ seems to influence the fragmentation path of ^{11}Be, ^{14}B, ^{17}C and ^{19}C for 1n-halo and ^{8}He, ^{11}Li, ^{12}Be, ^{14}Be and ^{19}B for 2n-halo significantly. However the lower angular momentum component up to $\ell = 4\hbar$ seems to play silent role as expected in reference to ground state decay observation in the 1n and 2n-halo systems. The deformation effects seem to be important for ^{22}O, ^{23}O, ^{24}O, ^{26}F, ^{29}Ne and ^{31}Ne in case of 1n-halo nuclear systems whereas the same seem to be contributing significantly for ^{17}B, ^{22}C, ^{23}N, ^{27}F and ^{29}F in case of 2n-halo category. The most interesting aspect of this study is that although PES are modified significantly with inclusion of deformation effects, but the 1n and 2n-halo status remains intact almost for all cases investigated here except for ^{17}B, ^{22}C and ^{29}F nuclei. It may be noted that deformation effects are included only up to quadrupole deformations in the present work.

In future, further work can be done in order to study the role of higher multipole deformations on these halo nuclei. In the present work all calculations have been done with the constant value of R_0 in radius (modified for deformation effects) but as we know all halo nuclei have much larger radius than it to be expected for a normal nucleus. So it will be of further interest to study the dynamics of these halo systems by taking more appropriate radii in order to have explicit understanding of structure mechanism and core configuration in these rare nuclei in light mass region. It may be relevant to mention here that use of these halo nuclei as projectile in loosely bound reactions [7-9] is one of the hot topic in nuclear reaction dynamics at low energy. Therefore the information contained in present work is of extreme relevance in reference to nuclear reaction dynamics and related phenomena at low energy. CCM based results are also shown for recently investigated 1n-halo ^{31}Ne nucleus showing ^{30}Ne core and 1n halo configuration.

References

[1] R. K. Gupta, Kumar S and Scheid W 1995 *J. Phys. G: Nucl. Part. Phys.* 21 L27

[2] R. K. Gupta, Balasubramaniam M, Puri R K and Scheid W 2000 *J. Phys. G: Nucl. Part. Phys.* 26 L23

[3] G. Audi and A.H. Wapstra and C. Thiboult, Nucl. Phys. A 729, 337(2003)

[4] Y. Urata, K. Hagino, and H. Sagawa Phys. Rev. C 83, 041303(R) (2011)

[5] W. Horiuchi, Y. Suzuki, P. Capel, and D. Baye, Phys. Rev. C 81, 024606 (2010).

[6] M. Takechi *et al.*, Nucl. Phys. A 834, 412c (2010).

[7] E. F. Aguilera et. al. Phys. Rev. C 79, 021601 (R) 2009.

[8] A. Lemasson et. al. Phys. Rev. Lett. 103, 232701 (2009).

[9] K. Tanaka et. al. Phys. Rev. Lett. 104, 062701 (2010).